Interaction Notes

Note 450

February 1983

ANALYTIC TREATMENT OF CABLE BUNDLES WITH LARGE NUMBERS OF COMPONENT WIRES

R. L. Gardner
J.L. Gilbert
L. Baker

Mision Research Corporation
1720 Randolph Rd. S.E.
Albuquerque, NM 87106

Abstract

In this report a method of calculating the electromagnetic response of cable bundels with large numbers of component wires is presented. Traditional methods of solving this problem usually use multiconductor transmission line theory. Use of multiconductor transmission line theory requires knowledge individual and mutual capacitances, conductances, resistances, and inductances per unit length of line. Limits on computer systems limit the multiconductor transmission line methods to about ten component cables. Cable bundles of interest have as many as 800 wires.

To solve this problem the corss section of the bundle is treated in a continuous variable aproximation and only the interaction of nearest neighbors is modeled. The continuous variable approximation is frequently used in mathematics when many discrete quantities that vary slowly with position are considered.

In addition, circuit theory is applied to treat various canonical problems in analysis of bundles are treated. The cases that are induced are: (1) removal of a wire from a bundle to include a sensor, (2) terminations, (3) branches in bundles and (4) departure of a bundle from a combed condition.

Of particular interest is the result for removal of a wire to add a sensor. In one configuration the fraction of the bundle current carried on this wire increased from 5 percent to 17 precent of the bundle current as the wire was removed.

CONTENTS

I. DISCUSSION

A driving uncertainty in determining a satellite's response to System-Generated Electromagnetic Pulse (SGEMP) is not knowing what currents are induced on complex cable bundles, and not knowing the distribution and magnitude of those currents. In some satellites these complex bundles consist of bulk wiring made up of large numbers of individually shielded wires (up to 800). Analyzing this problem is made difficult by the extremely large numbers of cables and the uncertainty of the geometric description of the bundle. That is, he location of an individual wire within a bundle may change from the exterior surface to the interior in some unknown way. Further, the location of the bundle relative to the satellite conducting surface, the cable terminations, and the details of the cable drive, are in general, not well known.

BOUNDS

One solution to this problem is to assume that the individual shield currents have bounds relative to the bulk cable currents. The bulk cable currents to some degree of approximation may be calculated. Empirically, the ratio I_{wire}/I_{cable} seems to be within $0.2 \leq I_{wire}/I_{cable} \leq 2$ (Ref. 1) for complex cable bundles on aircraft and satellites. In the aircraft case, however, individual wire currents are observed as much as 3.5 times the bulk current (Ref. 1), indicating that the empirical rule may hold some surprises. As a worst case example, the two wire plus ground system with only differential mode currents, has zero bulk cable current but a large wire current.

The worst case example is not likely to occur in the satellite cable system because exact differential drive is unlikely. Sources of differential modes that are likely to occur in satellites include differing sources for

individual cables, out of phase signals because of differing reflections from terminations and branches, and out of phase signals due to differing propagation velocities for individual wires. These mechanisms support a factor of two limit for the two wire bundle. The multiconductor transmission line is made up of the shields of the individual cables and ground. The terminations are, therefore, all shorts to ground. There are two major propagation velocities, i.e., those between wires and that for waves propagating along the exterior cables and ground.

OBSERVED UNCERTAINTIES

There are several results of the cable drive tests which are not completely understood. One is the distribution of shield currents over a bundle. For a bundle of about n = 45 shielded wires, all of the individual shield currents were measured 3 to 5 at a time. The peak shield currents were never less than about 30 percent of the bundle current, nor more than about 1.2 times the bundle current.* The currents are then generally equal to each other, but a substantial fraction of the bundle current each. For steady, in-phase currents evenly distributed along the perimeter of a bundle, each wire should carry $1/(\sqrt{n}) \approx .5$ percent of the bulk current. Since every wire carries much more current than the uniform distribution quantity, there is something not understood about the distribution of currents on a bundle and/or the measurement technique. It is possible the shield current is perturbed by pulling the shield being measured out of the bundle and installing a probe on the shield, even though pin current and voltage measurements with and without the current probe indicate this perturbation is small. The installation of the probes does cause the terminal impedance to be changed from a short-to-ground to about a 1-Ω impedance.

A second uncertainty is that of the dirve. The total bundle current (measured in-place in the FLTSATCOM tests) is about an order of magnitude smaller-than predictions assuming the bundle is a large conductor. These same rpedictions gave reasonable predictions for a simple cable bundle for the same capacitive drive. These two questions are addressed in this report.

*Ibid.

II. APPROACH

There are three problems addressed in this report

(1) Distribution of currents on a bundle of shielded wires

(2) Perturbation of measurements by sensors

(3) Explanation of differences in predictions for bulk currents for complex and simple bundles

Solution techniques are described in order.

CURRENT DISTRIBUTION

The main difficulty in analyzing bundles of cables with a large number of component cables is that, if each wire is treated individually, the analysis becomes extremely complex if the number of individual cables involved is more than about ten. Also, standard multiconductor cable theory requires knowledge of the bundle geometry to operate correctly. Such knowledge is not generally available, nor can the exact dimensions be expected to be maintained over time.

Therefore, what is needed is a theory which will provide estimates for cable currents for large bundles (perhaps hundreds of individual wires) as a function of position and which also consider branching, terminations, and lack of complete combing. When a large number of discrete quantities act in concert, a continuous variable approximation is more normally used. In this approximation, the wire bundle becomes a uniaxial cylinder. Propagation in the cylinder is developed here and the theory of driving the solutions is described in a later section.

PROPAGATION IN A UNIAXIAL CYLINDER

A uniaxial medium has a tensor conductivity, but that tensor is diagonal. In this case the tensor appears as

$$[\sigma] = \begin{bmatrix} \sigma & 0 & 0 \\ 0 & \sigma & 0 \\ 0 & 0 & \sigma_z \end{bmatrix} \tag{1}$$

with $|\sigma_z| >> |\sigma|$. $\sigma = g + i\omega e$ and $g = 0$ for this problem, but the imaginary part represents the capacitive coupling between wires.

Maxwell's equations for the uniaxial media case (Ref. 2)

$$\nabla \times \overline{H} = (\sigma)\,\overline{E} \tag{2}$$

$$\nabla \times \overline{E} = -i\omega(\mu)\,\overline{H} \tag{3}$$

The fields decouple if a Transverse Electric (TE), Transverse Magnetic (TM) basis is used. First, for TM, $H_z = 0$. Let

$$\overline{H} = \nabla \times \overline{A} \tag{4}$$

then

$$\nabla \times \nabla \times \overline{A} = (\sigma)\overline{E} \tag{5}$$

and

$$\nabla \times (\overline{E} + i\omega\mu\overline{A}) = 0 \tag{6}$$

or

$$\overline{E} + i\omega\mu\overline{A} = -\nabla\phi \tag{7}$$

so

$$\nabla \times \nabla \times \overline{A} + (\sigma)[\nabla\phi + i\omega\mu\overline{A}] = 0 \tag{8}$$

$$\nabla \times \nabla \times \overline{A} + \sigma\nabla\phi + i\omega\mu\sigma\overline{A} - (\sigma - \sigma_z)\frac{\partial\phi}{\partial z}\hat{z} - (\sigma - \sigma_z)i\omega\mu A_z\hat{z} = 0 \tag{9}$$

$$-\nabla^2\overline{A} + \nabla(\nabla \cdot \overline{A}) + \sigma\nabla\phi + i\omega\mu\sigma\overline{A} - (\sigma - \sigma_z)\frac{\partial\phi}{\partial z}\hat{z} - (\sigma\ \sigma_z)i\omega\mu A_z\hat{z} = 0 \tag{10}$$

Choose gauge

$$\nabla \cdot \overline{A} + \sigma\phi = 0 \tag{11}$$

This gauge is consistent with usual Lorentz gauge for

$$\sigma = g + i\omega\varepsilon \qquad g = 0 \tag{12}$$

Then

$$-\nabla^2\overline{A} + \gamma^2\overline{A} + \frac{(\sigma - \sigma_z)}{\sigma}\frac{\partial}{\partial z}(\nabla \cdot \overline{A}) - (\sigma - \sigma_z)\, i\omega\mu A_z\hat{z} = 0 \tag{13}$$

where

$$\gamma^2 = i\omega\mu\sigma \tag{14}$$

As is usual, all the fields may be derived from a potential

$$\overline{A} = (0,\ 0,\ A_z) \tag{15}$$

This assertion may be proved by directly deriving the potential equations from Maxwell's equations in component form. The result is that

$$A_z = -\frac{E_z}{\gamma^2 + \lambda^2} \tag{16}$$

if it is assumed that solutions are decomposed into a spectrum of plane waves, i.e., A_z, etc. proportional to $e^{-i\lambda z}$. The wave equation for the TM case is then

$$\nabla^2 A_z = \frac{(\sigma - \sigma_z)}{\sigma}\frac{\partial^2}{\partial z^2}A_z - \frac{\sigma_z}{\sigma}\gamma^2 A_z = 0 \tag{17}$$

For the case of $e^{-i\omega z}$, $e^{-i\lambda z}$ field variation this equation becomes

$$\frac{1}{\rho}\frac{\partial}{\partial\rho}\rho\frac{\partial}{\partial\rho}A_z - \frac{m^2}{\rho^2}A_z - (\gamma^2 + \lambda^2)\frac{\sigma_z}{\sigma}A_z = 0 \tag{18}$$

Solutions to this equation are

$$A_z = \begin{cases} I_m(u\rho)\, e^{-im\phi}\, e^{i\lambda z} \\ K_m(u\rho)\, e^{-im\phi}\, e^{-i\lambda z} \end{cases} \tag{19}$$

where

$$u^2 = \frac{\sigma_z}{\sigma}(\gamma^2 + \lambda^2) \tag{20}$$

The fields may be obtained from the potentials (Ref. 3)

$$E_\rho = \frac{\partial^2 A_z}{\partial\rho\partial z} \qquad H_\rho = \frac{\sigma}{\rho}\frac{\partial A_z}{\partial\phi}$$

$$E_\phi = \frac{\partial^2 A_z}{\rho\partial\phi\partial_z} \qquad H_\phi = -\sigma\frac{\partial A_z}{\partial\rho}$$

$$E_z = \left(-\gamma^2 + \frac{\partial^2}{\partial z^2}\right)A_z \qquad H_z = 0 \tag{21}$$

This is the TM case. For the TE case let

$$\overline{F} = \nabla \times \overline{E} \tag{22}$$

and duality provides the equation

$$\nabla^2\overline{F} = -\frac{(\mu - \mu_z)}{\mu}\frac{\partial}{\partial z}(\nabla \cdot \overline{F}) - \frac{\mu_z}{\mu}\gamma^2 F_z\hat{z} = 0 \tag{23}$$

with obvious solutions.

There are two important cases of coupling for this cable problem. The simplest is where the cable is excited by a concentric conduit. This case is ϕ independent and therefore uses only the zeroth order Bessel functions. The driving current density on the conduits may be Fourier decomposed, and is given by

$$j_{z,\phi} = \int_{-\infty}^{\infty} \begin{Bmatrix} f(\lambda) \\ g(\lambda) \end{Bmatrix} e^{-i\lambda z}\, d\lambda \tag{24}$$

The potential also may be decomposed

$$\begin{matrix} A_z \\ F_z \end{matrix} = \int_{-\infty}^{\infty} \begin{Bmatrix} M'(\lambda) \\ N'(\lambda) \end{Bmatrix} I_0\left(\frac{u}{v}\rho\right) \begin{Bmatrix} M''(\lambda) \\ N''(\lambda) \end{Bmatrix} K_0\left(\frac{u}{v}\rho\right) d\lambda \tag{25}$$

Obeying boundary conditions from the surface current on the driving cylinder, and at the boundary between air and the cable will determine the

unknown coefficients. Solution of the problem is then reduced to evaluation of a Fourier (albeit difficult) integral.

CONSTITUTIVE RELATIONS

Within the uniaxial cylinder the longitudinal conductivity are those of the shield. However, the coupling is capacitive in the transverse direction, which changes the equivalent permittivity and permeability for the medium. These quantities may be derived from a cylindrical version of the derivation of the dielectric constant from the molecular polarizability. Consider a conducting cylinder of radius a in a local uniform $\hat{z}$-directed electric field. The potential is

$$Q = \left(\rho - \frac{A}{\rho}\right) \cos \theta \tag{26}$$

where $A = a^2$ to preserve $\phi = 0$ at the surface of the cylinder. The normal electric field on the surface of the cylinder is

$$E_n = \nabla\phi = 2 \cos \theta \tag{27}$$

so there is a factor of 2 enhancement of the incident field. The surface charge density on the conducting cylinder is then

$$\sigma = 2\varepsilon_0 \cos \theta \tag{28}$$

The dipole moment per unit length is then formed by integrating the charge times the charge displacement

$$M = \int_0^{2\pi} 2\varepsilon_0 \cos \theta \ (a \cos \theta) \ a d\theta = 2\pi a^2 \varepsilon_0 \tag{29}$$

If the wires are packed with N wires per square centimeter, then the polarizability is

$$\chi_e = 2\pi N a^2 \varepsilon_0 \tag{30}$$

and the relative permittivity

$$\varepsilon_r = 1 + \frac{\chi_e}{\varepsilon_0} = 1 + 2\pi N a^2 \tag{31}$$

The volume per unit length excluded by N wires per square centimeter is

$$V_{ex} = N\pi a^2 \tag{32}$$

so the relative permittivity becomes

$$\varepsilon_r = 1 + 2V_{ex} \tag{33}$$

and the relative permeability is

$$\mu_r = (1 + 2V_{ex})^{-1} \tag{34}$$

thus preserving the velocity along the wires as c, for the vacuum dielectric case. If the wires are separated by a material dielectric, as in the FLTSATCOM case, then the relative permittivity must be adjusted accordingly.

This completes the formulation of the propagation solution. Numerical examples follow in Section VII. A time domain solution of the propagation problem is given in Appendix A.

III. JUNCTION CONDITIONS

The above conditions determine the current flow in the continuous representation of the cable bundle until a discontinuity is encountered. Discontinuities, in this case, include branches, terminations, and, in some sense, redistribution of wires within the bundle. The effects of each of these discontinuities may be calculated using a continuous variable approximation to the junction condition (Ref. 4) by computing the scattering matrix of the junction.*

Consider a three tube network in which a single bundle branches into two smaller bundles according to a mapping operator, M. M operates only on the coordinates and maps position r_1 in tube 1 to r_2 in tube 2 or r_3 in tube 3, depending on r_1. There are some restrictions on the mapping. First the area of tube 2 plus the area of tube 3 must equal that of tube 1 to conserve the total number of wires. Perimeters are not conserved in conserving areas. Therefore, sufficient wires (unit areas) must be mapped from the interior of tube 1 to fill out the perimeter of tubes 2 and 3. For example, the splitting of circular tube 1 into two semicircular tubes 2 and 3 is performed by

$$\vec{r}_2 = \vec{r}_1 \qquad 0 \leq \phi_1 < \pi$$

$$\vec{r}_3 = \vec{r}_1 \qquad \pi \leq \phi_1 < 2\pi \tag{35}$$

The center wire goes to the edge of tube 2. From the solution to the propagation equations (Eq. 24) we have $J_z(r,t) = \sigma E_z(r,t)$ and $\rho(r,t)$ resulting charge density from the continuity equation incident on the junction from tube 1. The reflected waves into the three tubes, which may be derived from Kirchhoff's Laws for the junction are needed. The charge density is related to the potential in a wire through $\nabla^2 V = \rho/\varepsilon_0$. The formal inverse of the

capacitance matrix C (similar to $-6b^2 C_{od} \nabla_\perp^2$ in operator form, i.e., CV = Q, where C_{od} is the capacitance between the wire of interest and one of its nearest neighbors, and b is one-half the wire spacing; C and the above differential operator are the same in that either operating on V yield Q. In one case V is a vector; in the other V is a continuous variable, the infinite dimensional extension of the vector V.) is the inductance matrix $v^2 L$. A formal inverse to the transverse Laplacian may be found by considering a formal operator L_{op} which must have the property

$$L_{op} \nabla^2 V = V \tag{36}$$

The solution is

$$L_{op} = \int dS' \, G(r,r') \tag{37}$$

where G is the solution of

$$\nabla^2 G(r,r') = \delta(r-r') \tag{38}$$

and where S' is the cross section of the appropriate tube. The operator approach is not necessary for those geometries that need numerical treatment since the scattering matrix may be found knowing the self-capacitance of each cell in the tube, without going through the operator step. Kirchhoff's Laws then require that the voltages for the simple connections are the same at both ends of the connection and the current into the connection must be balanced by a current flow out of the connection. Then

$$V(\vec{r}_1) = MV(\vec{r}_1) = V(M\vec{r}_1) \tag{39}$$

$$J(\vec{r}_1) = -MJ(\vec{r}_1) = -J(M\vec{r}_1) \tag{40}$$

In this symbology V and I are functions of position and are continuous. Let Y be an operator which converts V into J, i.e., J = YV. Note this operator must act on the local voltage. That is, the voltage on tubes 2 and 3, formed from MV, uses the characteristic admittance operator for those tubes. Since the characteristic admittance operator is proportional to $\int dS \, G$, the Green's function and integration surface for the correct tube must be used. The Green's function must obey the boundary conditions of the respective tube, requiring numerical solution of most problems. This formal problem may now be solved.

In matrix-operator form, Kirchhoff's Laws, for continuity of current and voltage, are

$$\begin{pmatrix} 1 & -1 \\ YZ_o & YZ_o \end{pmatrix} \begin{pmatrix} V \\ MV \end{pmatrix} = 0 \tag{41}$$

where Z_o is the impedance of free space, and is included to provide for a unitless matrix operator. The incident and reflected waves are related by

$$V^{tot} = V^{inc} + V^{ref} \tag{42}$$

$$J^{tot} = J^{inc} - J^{ref} \tag{43}$$

for all tubes. Then

$$\begin{pmatrix} 1 & -1 \\ YZ_o & YZ_o \end{pmatrix} \begin{pmatrix} V^{inc} \\ MV^{inc} \end{pmatrix} + \begin{pmatrix} 1 & -1 \\ -YZ_o & -YZ_o \end{pmatrix} \begin{pmatrix} V^{ref} \\ MV^{ref} \end{pmatrix} = 0 \tag{44}$$

or in the scattering matrix-operator form

$$\begin{pmatrix} V^{ref} \\ MV^{ref} \end{pmatrix} = - \begin{pmatrix} 1 & -1 \\ -YZ_o & -YZ_o \end{pmatrix}^{-1} \begin{pmatrix} 1 & -1 \\ YZ_o & YZ_o \end{pmatrix} \begin{pmatrix} V^{inc} \\ MV^{inc} \end{pmatrix} \tag{45}$$

Note that with proper selection of mapping function and characteristic admittance matrix both redistribution of wires within a bundle and terminations may be treated.

IV. APPLICATION TO SENSOR INSERTION

An immediate application of the above procedure is to determine the effect of pulling a wire out of the bundle and placing a sensor around the shield. Measurements have indicated that the phasing of the current on the wires is such that each individual shield carries a fifth to a third of the bundle current, minimum. For the phasing to be such that all 45 wires in the bundle to have large currents when measured, indicates there is some perturbation by the sensor.

A single example of how current may be increased is to consider a large bundle from which a single wire is split off, and all are terminated in a short to ground. The simple circuit modeling this arrangement, for the case that the shields (except that of the wire being pulled out) are assumed well connected within a bundle, is a large inductor branching into small and large inductors in parallel. The current will flow predominantly into the large inductor, i.e., the large wire. However, since the inductance of the wire scales as a log and the division of the current for the equal excitation case scales as the diameter of the bundle more current will flow on the small wire than would have flowed if the separation had not occurred. The applicability of this example is yet to be established,

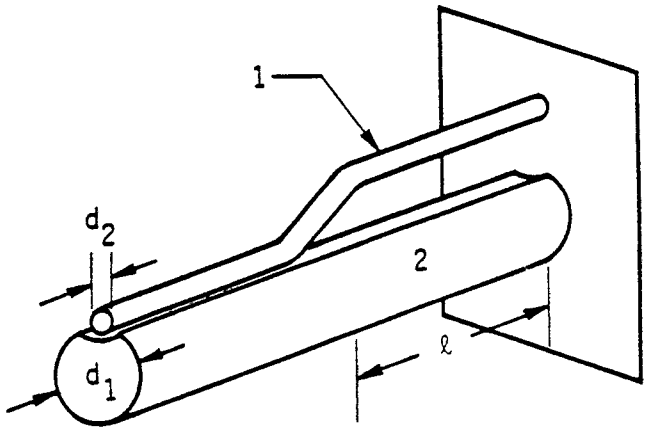

Figure 1. Geometry of a single wire pulled out of a bundle of wires.

since the electrical connectivity between wires is not as good as one might like. The connectivity will be considered later in a six-tube example.

Consider the breakout near the end of a cable bundle where one exterior wire is removed from the bundle, and consider the first reflection of the peak signal. If the wire is conductor 1 and the bundle is conductor 2, the capacitance matrix is, approximately, before the breakout

$$C_1 = \begin{pmatrix} \frac{C_b}{n} + C_m & -C_m \\ -C_m & C_b + C_m \end{pmatrix} \tag{46}$$

and, after the breakout

$$C_2 = \begin{pmatrix} C_s & 0 \\ 0 & C_b \end{pmatrix} \tag{47}$$

where C_b is the bundle over the ground plane, C_m is the mutual term between the wires, C_s is the capacitance of a single wire above the ground plane, and n is the number of perimeter wires. As a first approximation the mutual capacitance between the pulled out wire and the bundle are assumed zero. A better calculation of those mutuals is given in the next section. Consider frequencies low compared to the length over which the section is removed.

Specific example values for the coefficients, for a 49-wire bundle, are

$$\begin{aligned} \ell &= 5 \text{ cm} \\ \omega &= 10^8 \text{ s}^{-1} \\ d_1 &= 1.4 \text{ cm} \\ d_2 &= 0.2 \text{ cm} \\ n &= 22 \\ C_b &= 4 \times 10^{-11} \text{ F/m} \\ C_s &= 1.6 \times 10^{-11} \text{ F/m} \\ C_m &= 4 \times 10^{-10} \text{ F/m} \end{aligned} \tag{48}$$

and a typical bundle height is h = 2.4 cm. A useful figure of merit is $v/\omega\ell$ = 60, where v is the propagation velocity of a signal along the average transmission line. The velocity is assumed constant through the bundle.

The characteristic admittance of the wire before the breakout is

$$Y_1 = vC_1 \tag{49}$$

where v is the propagation velocity. The impedance of the breakout section is

$$Z_L = j\omega\ell L_2 \tag{50}$$

so the admittance is

$$Y_2 = \frac{v^2}{j\omega\ell} C_2 = \frac{v^2}{j\omega\ell} \begin{pmatrix} C_s & 0 \\ 0 & C_b \end{pmatrix} \tag{51}$$

Using these sign conventions

I_{ref} $\longrightarrow$

I_{trans} $\longrightarrow$

I_{inc} $\longrightarrow$

then the voltage and current must obey

$$V^i + V^r = V^t$$

$$I^i + I^r = I^t \tag{52}$$

The voltage and currents are related by

$$I^i = Y_1 V^i$$

$$I^r = -Y_1 V^r$$

$$I^t = Y_2 V^t \tag{53}$$

Solving these equations leads to

$$V^t = 2(Y_1 + Y_2)^{-1} Y_1 V^i$$

$$I^t = 2Y_2(Y_1 + Y_2)^{-1} Y_1 V^i \tag{54}$$

The useful V^i is

$$V^i = \begin{pmatrix} V_0 \\ V_0 \end{pmatrix} \tag{55}$$

representing a uniform excitation.

Substituting the appropriate values of the admittance matrices into the above equations

$$I^i = Y_1 V^i = v V_0 \begin{pmatrix} C_b/n \\ C_b \end{pmatrix} \tag{56}$$

and

$$(Y_1 + Y_2)^{-1} = \frac{1}{v\Delta} \begin{pmatrix} C_b + C_m + \frac{vC_b}{j\omega\ell} & C_m \\ C_m & \frac{C_b}{n} + C_m + \frac{vC_s}{j\omega\ell} \end{pmatrix} \tag{57}$$

where

$$\Delta = \frac{C_b^2}{n} + C_bC_m + \frac{C_bC_m}{n} + \frac{v}{j\omega\ell} \quad C_sC_b + C_sC_m + \frac{C_b^2}{n} + C_bC_m \quad + \frac{v^2C_sC_b}{(j\omega\ell)^2}$$

Finally, the transmitted current vector is

$$I^t = \frac{2vV_o}{\Delta} \frac{v}{j\omega\ell} \begin{pmatrix} \frac{C_sC_b^2}{n} + \frac{C_mC_bC_s}{n} + \frac{vC_b^2C_s}{j\omega\ell n} + C_bC_mC_s \\ \frac{C_b^2C_m}{n} + \frac{C_b^3}{n} + C_mC_b^2 + \frac{vC_sC_b^2}{j\omega\ell} \end{pmatrix} \tag{58}$$

A couple of cases are of interest. If $C_m \to 0$, (i.e, there is no mutual coupling) and the terms ordered are

$$C_b \gg C_s \gg \frac{C_b}{n} \tag{59}$$

then the transmitted current is

$$I^t = 2vV_0 \begin{pmatrix} C_b/n \\ C_b \end{pmatrix} = 2I^i \tag{60}$$

or the transmitted current is twice the incident current, which is pleasing.

In the ordering $C_m \gg C_b \gg C_s \gg C_b/n$, the transmitted wave is (if $C_m \gg vC_s/j\omega\ell$) for the tightly coupled bundle case

$$I^t = 2vV_o \begin{pmatrix} C_s \\ C_b \end{pmatrix} \tag{61}$$

The numerical example is

$$\frac{v}{\omega\ell} C_s > C_m > C_b > C_s > \frac{C_b}{n} \tag{62}$$

with

$$C_m > \frac{v}{\omega\ell} \left(\frac{C_b}{n}\right) \tag{63}$$

and the dominant terms turn out to be

$$I^t = 2vV_o \begin{pmatrix} \frac{j\omega\ell\ C_m}{v} \\ C_b \end{pmatrix} \tag{64}$$

The fraction of current on the single wire is

$$\frac{\omega\ell\ C_m}{v\ C_b} \approx 0.17 \tag{65}$$

For a uniformly excited bundle, each perimeter wire carries a current of about 0.05 of the bundle current. So even this approximation suggests a factor of 3.7 increase in the current on the wire.

Confirming this limiting estimate, a calculation of the current split using Equation 54 was performed for frequencies between 1 and 100 MHz. The result is shown in Figure 2.

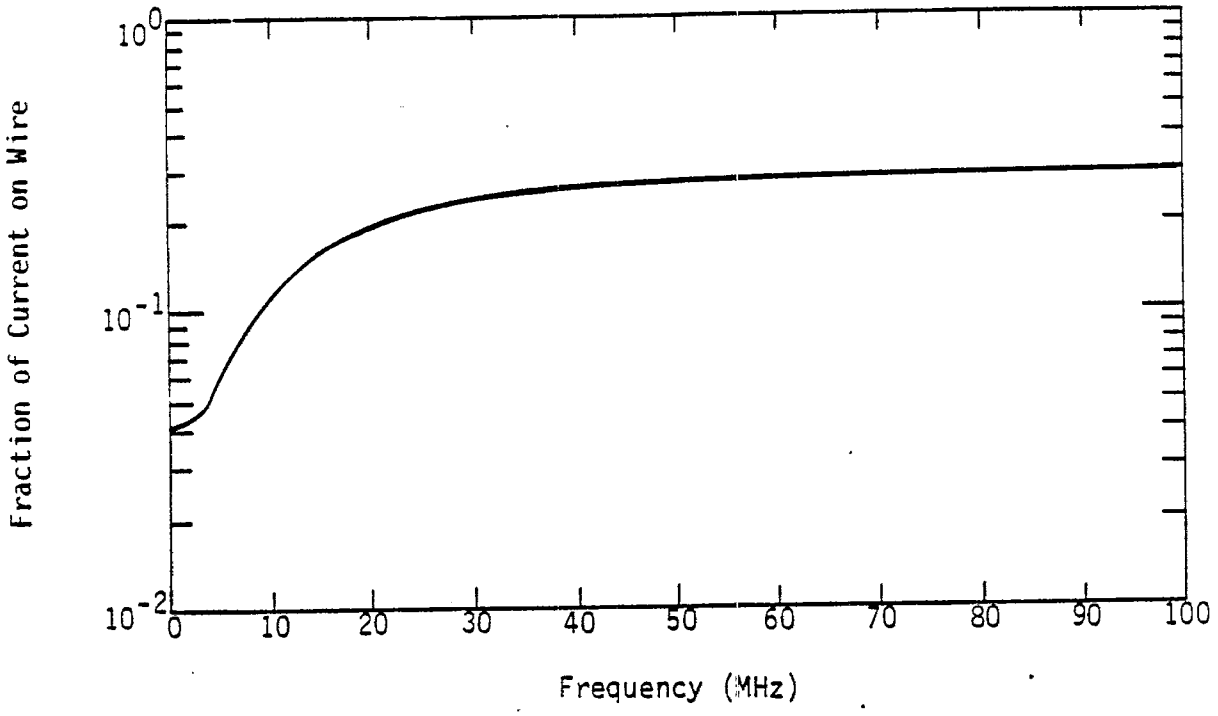

Figure 2. Current division as a function of frequency for the simple 4-tube case.

To illustrate that the splitting of the current from the bundle to the single wire occurs for a specific waveform, a power spectrum weighted average was carried out. Consider the current on the single wire as the product of a transfer function $T(\omega)$ and a bulk current $I(\omega)$. Then a power spectrum weighted average of the fraction F of the bulk current on the single wire is given by:

$$F^2 = \frac{\frac{R}{2\pi} \int_{-\infty}^{\infty} T^*(\omega)\, T(\omega)\, I^*(\omega)\, I(\omega)\, d\omega}{\frac{R}{2\pi} \int_{-\infty}^{\infty} I^*(\omega)\, I(\omega)\, d\omega} \tag{66}$$

where R is a characteristic, constant resistance.

For a generic cable drive test, a cable bundle was excited by driving a plate (1 m long and a few centimeters wide) parallel to the satellite ground plane with a voltage across the plate and a termination impedance at the center of the plate. The plate's long dimension ran along the cable.

The current for this calculation was assumed to be proportional to dV/dt, where V is the voltage applied to the parallel plate for the cable drive. The waveform used for the applied electric field was developed from the following curve fit:

$$E_p = 2.25 \times 10^5 \frac{e^{-\alpha t}}{1 + Ge^{-\beta t}} - \frac{e^{-\gamma t}}{1 + Ge^{-\delta t}} \qquad (67)$$

where

$$\alpha = 2 \times 10^9$$

$$\beta = \gamma = 2 \times 10^8$$

$$\delta = 2 \times 10^9$$

$$G = 1/(\beta/\alpha - 1)$$

The resulting waveform is shown in Figure 3. The result of this averaging process was that 16 percent of the bulk current (F) was shifted to the wire pulled out of the bundle, a factor of 3 more than one would expect for the uniform excitation case.

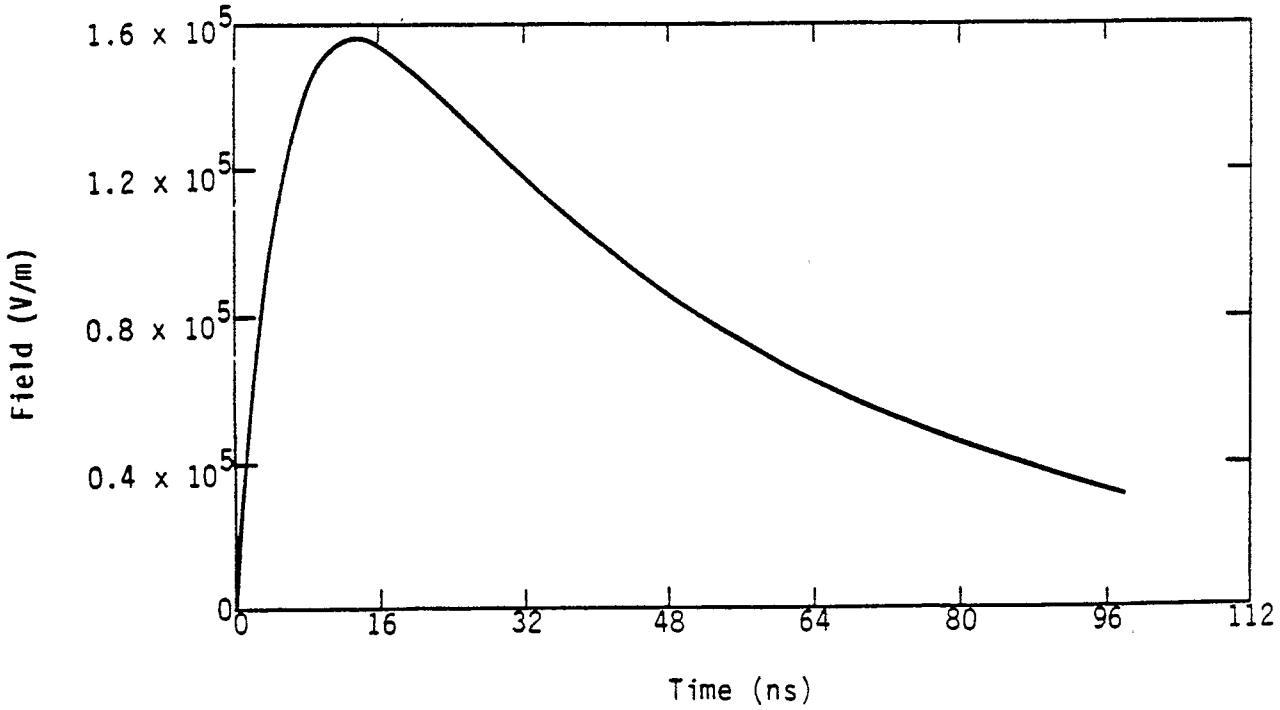

Figure 3. Waveform used for the weighted average of the current split off onto the small wire.

EFFECT OF MUTUAL TERMS ON CURRENT REDISTRIBUTION

The expression for C_2 in Equation 47 ignores the contribution of the capacitance between the bundle and the wire pulled out. An estimate of the mutual capacitance may be found by computing the elastance matrix for the following geometry by image theory and inverting the matrix to find the capacitance matrix. The geometry used for the image theory calculation is shown in Figure 4. As shown, only six image charges are used in the calculation.

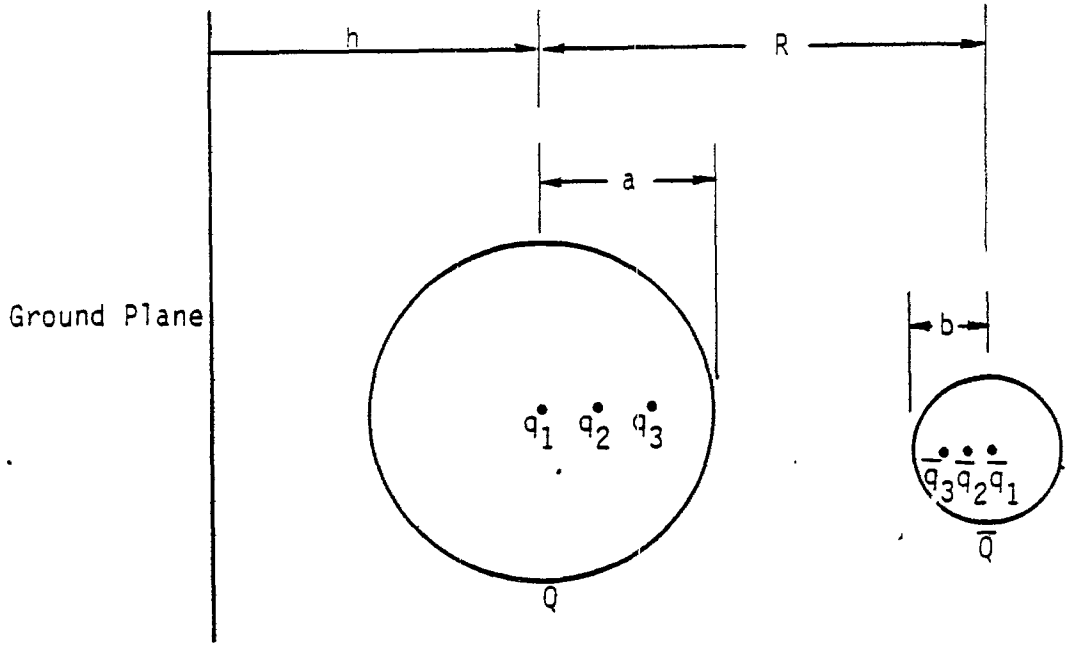

Figure 4. Image theory solution geometry.

If charges Q and $\bar{Q}$ are placed on the large and small cylinders in Figure 4, then the resulting potentials can be used to calculate the elastance matrix elements. The charges q_1 and $\bar{q}_1$ are located at the center of each of the cylinders and are used to control the total charge on each of the cylinders. q_2 is the image of $\bar{q}_1$ in the surface of the bundle. q_3 is the image of $\bar{q}_2 + \bar{q}_3$ in the surface of the bundle. Similarly, $\bar{q}_2$ and $\bar{q}_3$ are chosen to maintain a uniform potential on the surface of the wire. Note that the image theory series is truncated by assuming $q_2 + q_3$ generates only one image. A complete solution is an infinite series of image charges, so this solution is best when the separation between bundle and wire is more than a wire radius.

A numerical solution is required for better calculation of the capacitance matrix. Numerical treatment is required since the wire actually enters the bundle when it gets close. Further, the bundle is not a conductor but is a collection of capacitively coupled conductors.

The equations that the charges must obey are found by demanding that the image plus impressed charge contributions result in a uniform potential around the cylinder surface (Ref. 5). The equations are:

$$q_1 + q_2 + q_3 = Q \qquad \bar{q}_1 + \bar{q}_2 + \bar{q}_3 = \bar{Q}$$

$$q_2 = -\frac{a}{R}\bar{q}_1 \qquad \bar{q}_2 = -\frac{bq_1}{R}$$

$$q_3 = -\frac{a(\bar{q}_2 + \bar{q}_3)}{R - b^2/R} \qquad \bar{q}_3 = -\frac{b(q_2 + q_3)}{R - a^2/R} \tag{68}$$

If

$$\bar{K}_1 = ab\left(\frac{1}{R^2} - \frac{1}{R(R - a^2/R)}\right) \tag{69}$$

and

$$\bar{K}_2 = \left(1 + ab\left(\frac{1}{R(R - b^2/R)} - \frac{1}{(R - a^2/R)(R - b^2/R)}\right)\right) \tag{70}$$

then

$$\bar{q}_1 = -\frac{b/R\ Q - \bar{K}_2\bar{Q}}{R_1 - R_2} \tag{71}$$

and

$$K_1 = ab\left(\frac{1}{R^2} - \frac{1}{R(R - b^2/R)}\right) \tag{72}$$

$$K_2 = \left(1 + ab\left(\frac{1}{R(R - a^2/R)} - \frac{1}{(R - a^2/R)(R - b^2/R)}\right)\right) \tag{73}$$

$$q_1 = -\frac{a/R\ \overline{Q} - K_2 Q}{K_1 - K_2} \tag{74}$$

The other charges are found from

$$q_2 = -\frac{a}{R}\overline{q}_1 \tag{75}$$

$$q_2 = -\frac{\overline{b}\ q_1}{R} \tag{76}$$

$$\overline{q}_3 = \frac{\left(\frac{-bq_2}{R - a^2/R} + \frac{ab}{(R - a^2/R)(R - b^2/R)}\overline{q}_2\right)}{1 - \frac{ab}{(R^2 - a\ /R)(R^2 - b\ /R)}} \tag{77}$$

and

$$q_3 = -\frac{a}{R - b^2/R}(\overline{q}_2 + \overline{q}_3) \tag{78}$$

Finally, the locations of the charges are also determined by the boundary conditions (Ref. 5). For a coordinate system centered at the center of the bundle and the x-axis through the center of the wire, the locations are:

$$x_1 = 0$$

$$x_2 = a^2/R$$

$$x_3 = a^2/(R - b^2/R)$$

$$x_4 = R - b/(R - a^2/R)$$

$$x_5 = R - b^2/R$$

$$x_6 = R \qquad (79)$$

where the charges were reindexed to $q_{1,2,3} = \bar{q}_{1,2,3}$ and $q_4 = \bar{q}_3$, $\bar{q}_5 = \bar{q}_2$, and $q_6 = \bar{q}_1$.

The elastance matrix elements are then found by adding up the contributions of the various line charges to the potential at the surface of the bundle and wire.

The distances from the bundle surface for each of the charges are

$$d_1 = a$$

$$d_2 = a - a^2/R$$

$$d_3 = a - a^2/(R - b^2/R)$$

$$d_4 = R - a - b^2/(R - a^2/R)$$

$$d_5 = R - a - b^2/R$$

$$d_6 = R - a \qquad (80)$$

The distances from the wire surface

$$e_1 = R - b$$

$$e_2 = R - b - a^2/R$$

$$e_3 = R - b - a^2/(R - b^2/R)$$

$$e_4 = b - b^2/(R - a^2/R)$$

$$e_5 = b - b^2/R$$

$$e_6 = b \tag{81}$$

The elastance matrix elements are then:

$$Q = 0 \qquad \overline{Q} = 1$$

$$P_{11} = -\frac{1}{2\pi\varepsilon_o}\left[\sum_{i=1}^{6} q_i \ell n\, d_i - \ell n[2(h+R)]\right]$$

$$P_{21} = -\frac{1}{2\pi\varepsilon_o}\left[\sum_{i=1}^{6} q_i \ell n\, e_i - \ell n[2h+R]\right]$$

$$Q = 1 \qquad \overline{Q} = 0$$

$$P_{12} = -\frac{1}{2\pi\varepsilon_o}\left[\sum_{i=1}^{6} q_i \ell n\, d_i - \ell n[2h+R]\right]$$

$$P_{22} = -\frac{1}{2\pi\varepsilon_o}\left[\sum_{i=1}^{6} q_i \ell n\, e_i - \ell n[2h]\right] \tag{82}$$

where the additional logarithmic terms account for reflection in the ground plane.

The elastance matrix in Equation 82 was used in the calculation of C_2 above as a function of separation distance. Otherwise the problem was the same as that described in the previous section. The current division as a function of separation distance of the bundle and wire (surface to surface distance) is shown in Figure 5. Near the bundle the pulled out wire arries about 5 percent of the current, as it should. Farther from the bundle, for 100 MHz in particular, the fraction of current transferred to the wire becomes larger, reaching 21 percent of the total current. Both self and mutual capacitances are calculated with the image theory technique.

To confirm the conclusion of the effect of pulling out the wire two more geometries were treated using the same junction theory technique. The first of these geometries addresses the assumption that the bundle is a solid conductor and is shown in Figure 6.

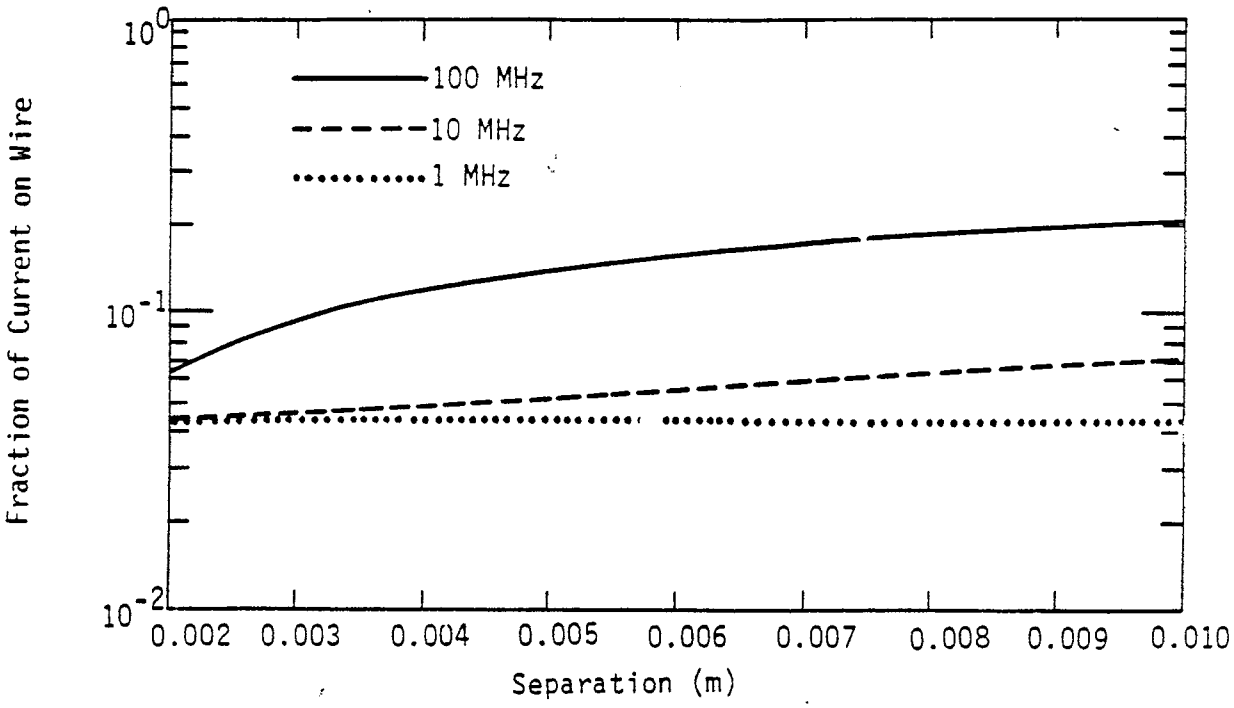

Figure 5. Current division for various frequencies as a function of the separation of the surfaces of the bundle and wire.

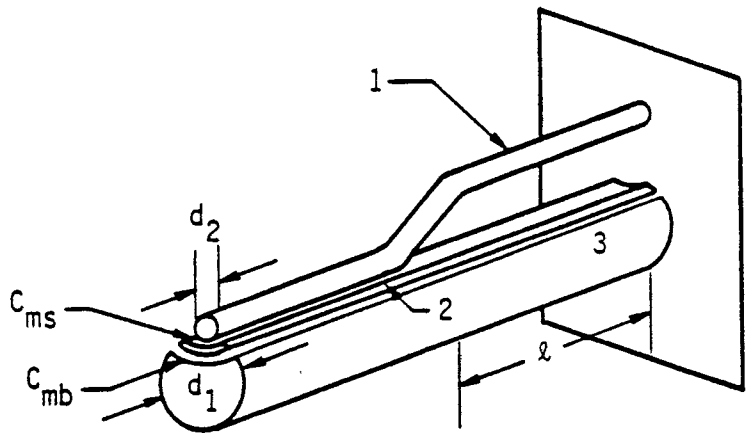

Figure 6. Modification of geometry in Figure 1 showing additional 3-wire section which allows first order treatment of the capacitive (rather than conductive) coupling between the wires in the bundle.

This problem is now a junction of three conductors and the capacitance matrix corresponding to those in Equation 46 is

$$C_1 = \begin{pmatrix} C_b/n + C_{ms} & -C_{ms} & 0 \\ -C_{ms} & 2C_b/n + C_{mb} + C_{ms} & -C_{mb} \\ 0 & -C_{mb} & (n-3)/n\ C_b + C_{mb} \end{pmatrix} \quad (83)$$

where C_1 represents the capacitance matrix before the junction, and as shown in Figure 6, C_{ms} and C_{mb} are the mutual capacitances between the intermediate layer and the wire and the bundle and intermediate layer respectively. After the junction the capacitance between the wire and intermediate layer is assumed negligible but the mutual capacitance between the layer and the bundle is unchanged. The resulting capacitance matrix after the junction is:

$$C_2 = \begin{pmatrix} C_s & 0 & 0 \\ 0 & 2C_b/n + C_{mb} & -C_{mb} \\ 0 & -C_{mb} & (n-3)/n\ C_b + C_{mb} \end{pmatrix} \quad (84)$$

Figure 7 shows the variation with frequency of the fraction of the total current that is shifted from the wire. At frequencies associated with the rise time of SGEMP or electric drive pulses a substantial fraction of the total current is shifted to the wire with the sensor. The effect is similar for this geometry to that for the 2 x 2 (or 4 tube) problem.

A final geometry is shown in Figure 8 which has two sensor wires pulled out in the same way from a bundle of 45 wires (22 surface wires). In this case the initial capacitance matrices where the bundle wire mutual capacitance is C_m.

$$C_1 = \begin{pmatrix} C_b/n + C_m & 0 & -C_m \\ 0 & C_b/n + C_m & -C_m \\ -C_m & -C_m & C_b + 2C_m \end{pmatrix} \quad (85)$$

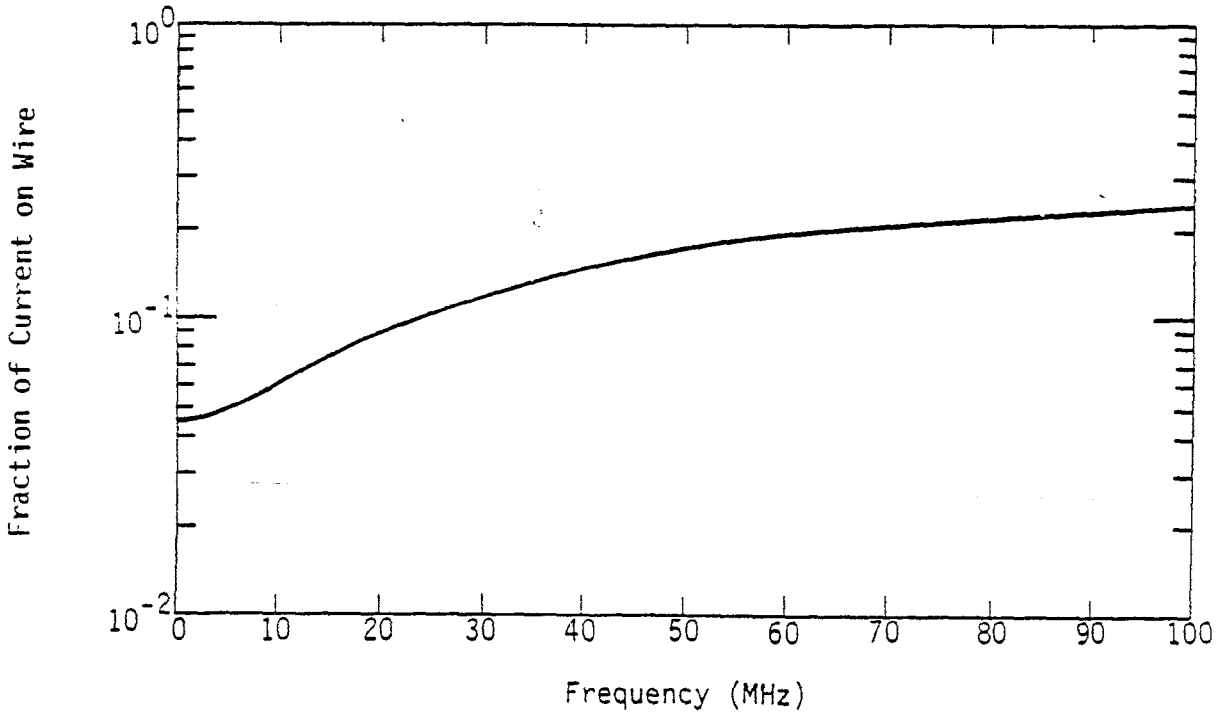

Figure 7. Fraction of bundle current flowing on single wire pulled out from the bundle for the case of the wire and nearest neighbors treated as tubes separate from the main bundle.

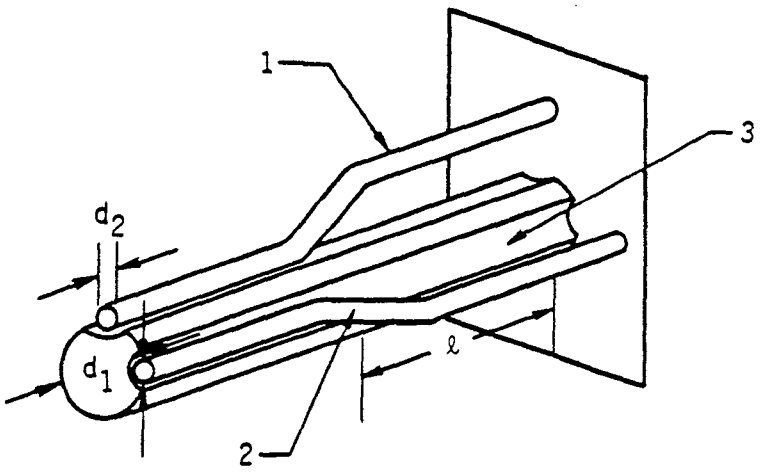

Figure 8. Geometry showing two wires pulled out of the bundle.

and

$$C_2 = \begin{pmatrix} C_s & 0 & 0 \\ 0 & C_s & 0 \\ 0 & 0 & C_b \end{pmatrix} \tag{86}$$

The fraction of the total current on each of the two wires is shown in Figure 9.

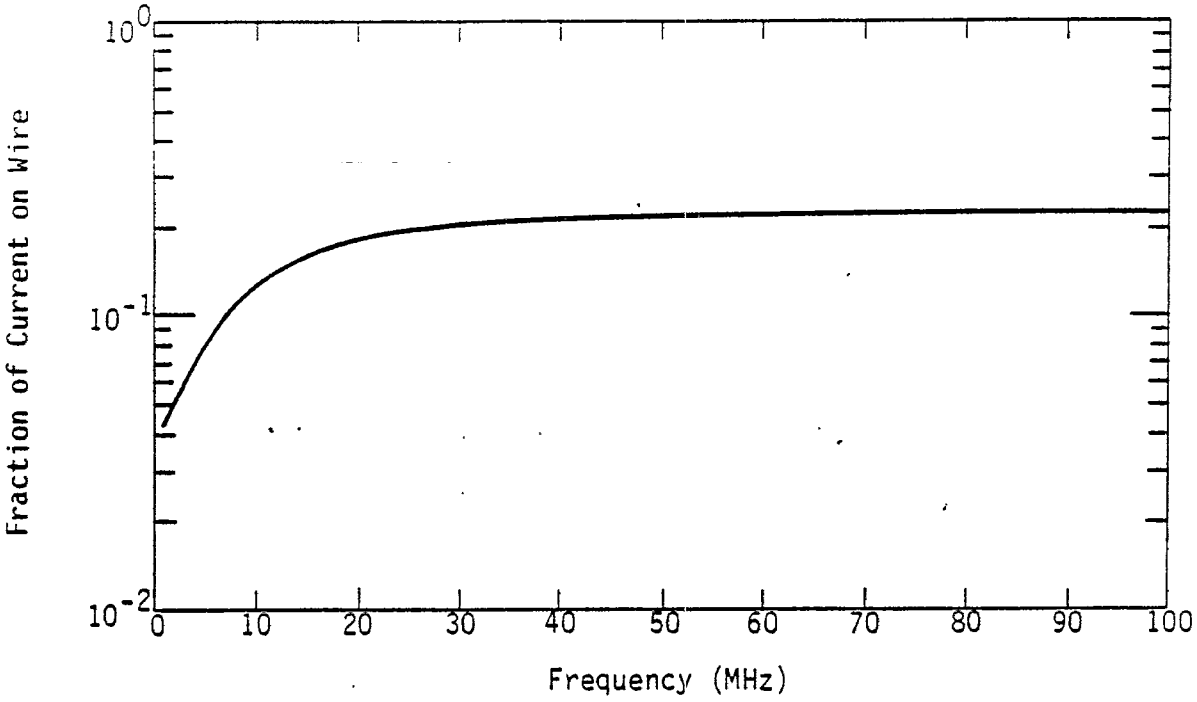

Figure 9. Fraction of bundle current flowing on each of two wires pulled out from the main bundle.

V. EFFECT OF A WIRE MOVING FROM THE OUTSIDE OF A CABLE BUNDLE TO THE INSIDE

An abrupt change in wire location is now considered. That is, the wire is moving from the outside of the cable bundle to the center of the cable bundle. A more gradual change would have less effect but would be more difficult to treat. Consequently, this is a limiting case.

Figure 10 shows how the exterior wire case is approximated.

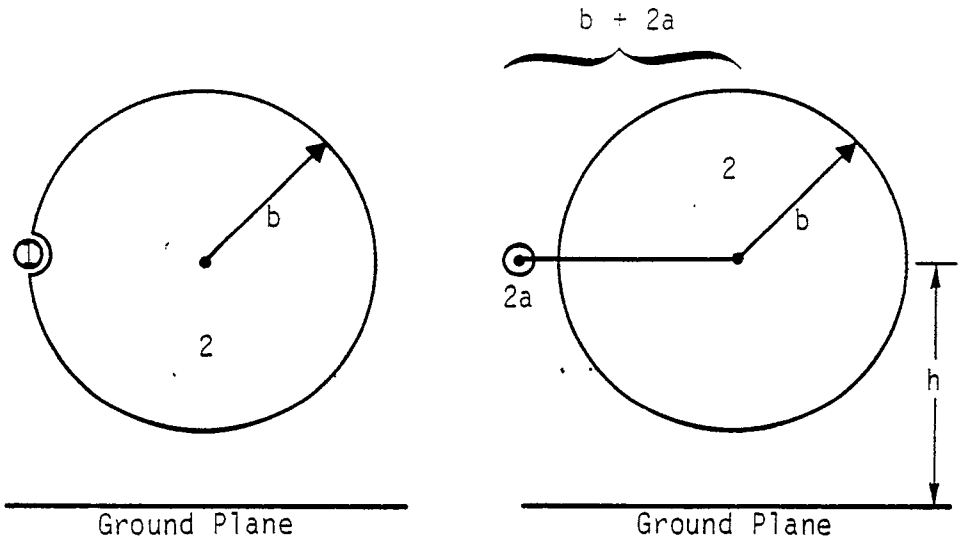

Figure 10. Sketch showing the approximate treatment of a wire on the surface. The exact geometry is shown on the left, the approximate geometry on the right.

The capacitance matrix is then approximately:

$$C_1 = \begin{pmatrix} C_g + C_m & -C_m \\ -C_m & C'_g + C_m \end{pmatrix} \tag{87}$$

where the capacitances to the ground plane for the wire and bundle are:

$$C_g = \frac{2\pi\varepsilon}{\log\left[\frac{h}{a} + \sqrt{\left(\frac{h}{a}\right)^2 - 1}\right]}$$

$$C'_g = \frac{2\pi\varepsilon}{\log\left[\frac{h}{b} + \sqrt{\left(\frac{h}{b}\right)^2 - 1}\right]} \tag{88}$$

while the mutual capacitance between the cylinders is given in Reference 6 as

$$C_m = \frac{2\pi\varepsilon}{\cosh^{-1}\psi_1 + \cosh^{-1}\psi_2} \tag{89}$$

where, with $p \equiv a/b$, $\psi_2 = (4+5p)/(2+4p)$, $\psi_1 = 1+3/4p$ (note that Eq. 36 on page 28 of Ref. 6 contains misprints in the subscripts for the a_i in the denominators).

For the wire at the center of the cable it is assumed that nearby wires form a cage around the central wire. Reference 6 shows that they may be treated as a cylindrical conductor with good accuracy. The central conductor is shielded effectively from the ground plane and other wires and gives

$$C_2 = \begin{pmatrix} C'_m & -C'_m \\ -C'_m & C'_m + C'_g \end{pmatrix} \tag{90}$$

for the capacitance matrix with C_g the same as before (Eq. 88) and

$$C'_m = \frac{2\pi\varepsilon}{\ell n \frac{r_{out}}{a}} \simeq \frac{2\pi\varepsilon}{\ell n(2)} \tag{91}$$

for uniform wire diameter. Then

$$I^t = 2Y_2 \left(Y_1 + Y_2\right)^{-1} Y_1 V \tag{92}$$

(notation as shown in Eq. 53) with $Y = vC$, and common-mode conditions of equal excitation:

$$V = \begin{pmatrix} V_0 \\ V_0 \end{pmatrix} \tag{93}$$

The incident current is

$$I^i = Y_1 V = vV_0 \begin{pmatrix} C_g \\ C'_g \end{pmatrix} \tag{94}$$

and the transmitted current is

$$I^t = vV_0 \vec{AQ} \tag{95}$$

with

$$A = \frac{2}{2C_g C'_g + (2C_g + C'_g)(C_{mt} + C'_m)} \tag{96}$$

$$\vec{Q} = \begin{pmatrix} C_g C'_g C_m \\ C'_g[C_g C_m C_g C'_g + C'_g(C_m + C'_m)] \end{pmatrix} \tag{97}$$

I^t/I^i is then a vector

$$\frac{I^t}{I^i} = A \cdot \begin{pmatrix} C'_g C_m \\ C_g C_m + C_g C'_g + C'_g(C_m + C'_m) \end{pmatrix} \tag{98}$$

$$\equiv AQ'$$

Using the same parameters for the 49-wire bundle,

$$\begin{aligned} a &= 0.2 \text{ cm} \\ b &= 1.4 \text{ cm} \\ h &= 5.0 \text{ cm} \end{aligned} \tag{99}$$

gives

$$\begin{aligned} C_g &= 1.4 \times 10^{-11} \text{ F/m} \\ C'_g &= 2.8 \times 10^{-11} \text{ F/m} \\ C_m &= 3.15 \times 10^{-11} \text{ F/m} \\ C'_m &= 8.0 \times 10^{-11} \text{ F/m} \end{aligned} \tag{100}$$

With these capacitances:

$$A = 0.028 \times 10^{22}$$

$$Q' \equiv \begin{pmatrix} 8.882 \times 10^{-22} \\ 39.55 \times 10^{-22} \end{pmatrix} \tag{101}$$

Thus, the ratio of transmitted to incident current is only 25 percent for the wire; it is 111 percent for the bulk of the cable, due to reflection at the impedance mismatch. The reflected waves are then 75 percent and -11 percent of the incident currents on this system. As expected, there is a great effect (reduction) on the wire current; the effect on the bundle is much less. Energy is conserved; the factor of 111 percent is due to an overreflection similar to the doubling of voltage upon reflection at an open circuit (infinite impedance or zero admittance). Similarly, the decrease in admittance as the wire moves to the center of the bundle results in a reflected wave on the bulk of the cable which increases its transmitted current.

This result should not be unexpected in light of the existing theory of multiconductor transmission lines. Reference 7 discusses how the common-mode admittance of a central conductor is generally smaller than the others. Therefore, the admittance of the wire should be expected to decrease, and this is indeed the result obtained. This results in significant wave reflection. Indeed, the common mode admittances are

$$Y_1^{cm} = vC_1 \begin{pmatrix} 1 \\ 1 \end{pmatrix} = v \begin{pmatrix} C_g \\ C_g' \end{pmatrix} \tag{102}$$

before and

$$Y_2^{cm} = v \begin{pmatrix} 0 \\ C_g' \end{pmatrix} \tag{103}$$

afterward, in the approximation of effective shielding by the inner ring of wires of the bundle. This accounts for the large effect on current transmitted through the junction between outer and inner wire.

VI. EFFECT OF SPLITTING OF A CABLE BUNDLE INTO TWO SMALLER BUNDLES

This section considers the effect of splitting the cable bundle into two smaller bundles on the transmitted currents in the common-mode. An equal division of the cable bundle is treated, but this may just as easily be the generalized case of unequal bundle splitting. The model is sketched in Figure 11.

Before the split, the cable halves are treated as D-shaped elements. Clearly, the shielding effects of the wires cause the major contribution to the mutual capacitance to be due to the wires on the flat sides of the D elements.

The capacitance matrix is

$$C_1 = \begin{pmatrix} C_m + C_g & -C_m \\ -C_m & C_m + C_g \end{pmatrix} \tag{104}$$

with

$$C_m = \frac{\varepsilon b}{d}$$

$$C_g = \frac{2\pi\varepsilon}{\log\left[\frac{h}{b} + \sqrt{\left(\frac{h}{b}\right)^2 - 1}\right]} \tag{105}$$

where

d = effective D separation

b = bundle radius

h = height above ground plane

a = wire radius

and $d \approx 2a/k$ where k = insulation dielectric constant. This result may be obtained by treating the system as sketched. From the definition of the

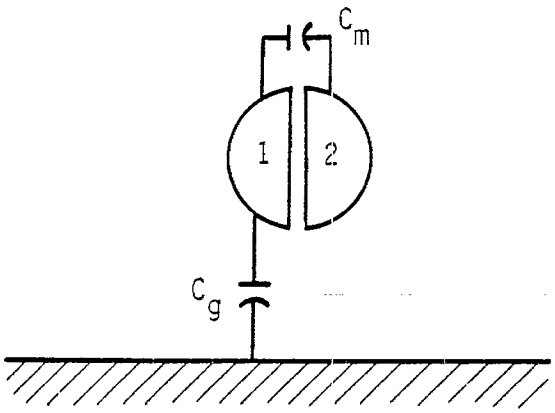

a. Before cable bundle is split.

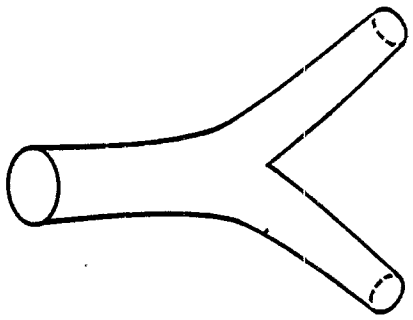

b. After cable bundle is split (top view).

Figure 11. Geometry of an equally split cable bundle. Before the split the two halves of the cable are treated as D shaped sections with the split normal to the ground plane. The terms in the capacitance matrix are shown.

capacitance matrix there are two parallel capacitors between bundle half 1 and the ground: C_m between the two halves and C_g to the ground plane.

In computing C_g, the D-shaped half-bundle is treated as though it were a circular cross section. After the splitting of the bundle halves, we have,

$$C_2 = \begin{pmatrix} C'_g & 0 \\ 0 & C'_g \end{pmatrix} \tag{106}$$

where the mutual interaction of the bundles is neglected, as though they are almost orthogonal and distant, with

$$C'_g = \frac{2\pi\varepsilon}{\log\left[\frac{h'}{b'} + \sqrt{\left(\frac{h'}{b'}\right)^2 - 1}\right]} \simeq \frac{2\pi\varepsilon}{\log \frac{2\sqrt{2}h}{b}} \tag{107}$$

where h is assumed to be unchanged but each bundle now has been halved in cross section (radius is smaller by a factor of $\sqrt{2}$).

The admittances matrix is

$$Y = vC \tag{108}$$

where v is the wave velocity. The transmitted current

$$I^t = 2Y_2 (Y_1 + Y_2)^{-1} Y_1 V^i \tag{109}$$

In the common-mode case

$$V^i = \begin{pmatrix} V_0 \\ V_0 \end{pmatrix} \tag{110}$$

Therefore, the results for each bundle half are identical,

$$I^t = vV_0 A$$
$$A = \frac{2C'_g(C_g^2 + C_g C'_g + 2C_g C_m)}{C_g^2 + C_g'^2 + 2(C_m C_g + C_g C'_g + C_m C'_g)} \tag{111}$$

Because $I^i = vV_0 C_g$,

$$\frac{I^t}{I^i} = A/C_g \tag{112}$$

Using the same parameters used for the 49-wire bundle (Eq. 99): a = 0.2 cm, b = 1.4 cm, h = 5 cm; gives

$$C_m = 6.2 \times 10\text{-}11 \text{ F/m}$$

$$C_g = 2.8 \times 10^{-11} \text{ F/m}$$

$$C'_g = 2.4 \times 10^{-11} \text{ F/m}$$

$$I^t = 1.07\ vV_0 C'_g$$

$$\frac{I^t}{I^i} = 1.07\ \frac{C'_g}{C_g} = 0.92 \qquad (113)$$

or a slight reduction in transmitted current.

VII. COUPLING TO COMPLEX VERSUS SIMPLE BUNDLES

It has been observed that simple theory of a conductor in a capacitive drive predicts reasonable bulk currents on the FLTSATCOM demonstration test geometry, but give an order of magnitude to high current predicitons on the actual FLTSATCOM geometry. More precisely several amps were induced on the cable bundle in the demonstration test from a 1.5 kV pulsar and 1 to 2 A were induced on the qualification model test using a 4 kV pulsar. The demonstration test geometry consists of one large coaxial cable surrounded by a few hook-up wires. The equivalent FLTSATCOM test geometry consists of about two hundred small shielded cables. The physical difference in the three geometries is their ability to support azimuthal currents. The conductor and large coaxial cable support azimuthal currents on the exterior surface as well as they support longitudinal currents. There is, however no conductive coupling between the wires in the FLTSATCOM case. The capacitive coupling is as described in the propagation section.

In a description of the excitation of the cable bundle there are two cases of interest. The first case is that of the induced current and voltage caused by a voltage applied to a coaxial cable surrounding the grounded cable shields. This example has the advantage of azimuthal symmetry and the complete decoupling of TE and TM modes on the line. The second case is that of a voltage applied to a plate centered above the cable bundle. This case is more complex than the case above but is closer to the excitation used in actual tests.

To get a feel for the problem, a limiting excitation case should be examined first. The length of the exciting plate is chosen so that the field variation along its length is small. So examination of the z-independent solution is enlightening. As above the fields may be derived from the potentials U and V through

TE	TM
$H_\rho^h = \frac{\partial^2 V}{\partial \rho \partial z}$	$E_\rho^e = \frac{\partial^2 U}{\partial \rho \partial z}$

$$H_\phi^h = \frac{\partial^2 V}{\rho \partial \phi \partial z} \qquad E_\phi^e = \frac{\partial^2 U}{\rho \partial \phi \partial z}$$

$$H_z^h = \left(-\gamma^2 + \frac{\partial^2}{\partial z^2}\right) V \qquad E_z^e = \left(-\gamma^2 + \frac{\partial^2}{\partial z^2}\right) U$$

$$E_\rho^h = -\frac{i\omega\mu}{\rho} \frac{\partial V}{\partial \phi} \qquad H_\rho^e = \frac{\sigma}{\rho} \frac{\partial U}{\partial \phi}$$

$$E_\phi^h = i\omega\mu \frac{\partial V}{\partial \rho} \qquad H_\phi^e = -\sigma \frac{\partial U}{\partial \rho}$$

$$E_z^h = 0 \qquad H_z^e = 0 \qquad (114)$$

where $\gamma^2 = i\omega\mu\sigma$ and U and V are the potentials for the TM and TE components of the fields. These are

$$U = \begin{pmatrix} I_m(u\rho) \\ K_m(u\rho) \end{pmatrix} e^{-im\phi} \, e^{-i\lambda z} \qquad (115)$$

where

$$u^2 = \frac{\sigma_z}{\sigma} \left(\gamma^2 + \lambda^2\right)$$

and

$$V = \begin{pmatrix} I_m(v\rho) \\ K_m(v\rho) \end{pmatrix} e^{-im\phi} \, e^{-i\lambda z} \qquad (116)$$

where

$$v^2 = \frac{u_z}{\mu} \left(\gamma^2 + \lambda^2\right)$$

and λ is a continuous variable describing the z-dependence of the fields. For the excitation problem, the electrical length of the driver was chosen by the experimentalists in such a way that the field variation along the driver is small. For $e^{-i\lambda z}$ behavior in z, the driver only allows significant contribution from λ small, within the driver. Near the ends of the driver this condition, of course, does not hold. The standard CV driver requires a contribution all along the cable length. For λ small

TE	TM
$H_z^h = -\gamma^2 V$	$E_z^e = -\gamma^2 U$
$E_\rho^h = -\frac{i\omega\rho}{\rho}\frac{\partial V}{\partial \rho}$	$H_\rho^e = \frac{\sigma}{\rho}\frac{\partial U}{\partial \phi}$
$E_\phi^h = -i\omega\mu\frac{\partial V}{\partial \rho}$	$H_\phi = -\sigma\frac{\partial U}{\partial \rho}$

(117)

All other components are 0 or are assumed negligible.

In the interior of the driver the driver may be specified in the problem by using a boundary condition of a constant electric field at some distance from the bundle. For a coaxial driver, the impressed E-field is $E = E_\rho\big|_{r=b}$ = constant. For the parallel plate system $E = E_x\big|_{r=b}$, say, would be an appropriate boundary condition for the driver. Conducting boundary conditions for the coaxial driver and continuity of tangential fields at the bundle surface complete specification of the problem. Note, however, that specification of E_ρ, and/or E_ϕ drives only the TE waves. The TM waves are not driven in the slow variation in the z case. However, the TE waves require that a J_ϕ exist at the surface of the conductor, since there is a nonzero E_ϕ required. Since J_ϕ can, at most, be a small displacement current on the actual cable bundle, the driven TE waves cannot easily propagate in the system but may propagate easily on the demonstration test bundle. This propagation restriction is supported in practice by waveguide filters, to get rid of, say, TM waves, constructed out of thin closely spaced spirals of insulated wire (Ref. 8). Further a more detailed calculation of the coaxial drive geometry shows that the impedance $Z_s = E_z/H_\phi\big|_{\rho=a}$, relating to TM (looking into the bundle along a radius vector) changes very little when the transverse conductivity is changed from the highly conducting value appropriate to the demonstration test to the $\sigma_t = i\omega\varepsilon_t$ case for the actual bundle. The arguments do not hold near the ends of the driver and the drive and mode conversion occurring there cause the currents that are driven on the real cable bundle.

For the TE case, however, the admittance

$$Y_s = - \frac{H_s}{E_\rho} \Bigg|_{\rho=a} \tag{118}$$

changes substantially for the σ_t change.

This same argument should also hold for the SGEMP excitation that is being simulated here.

There is also a difference of frequency content between the two test geometries. The first geometry has frequency content of about 40 to 60 MHz, while the second has a content of around 100 MHz, which is probably due to differing junction conditions in the two geometries. Following will be current distributions in ρ,z from the detailed model.

CABLE BUNDLES TESTS

Now considered is the application of the TM mode excitation model just developed to the specific case of the generic experiments. In these experiments, a cable consisting of a number of shielded wires was positioned between a drive plate and the wall of the satellite, which served as a ground plane. Such a geometry capacitively couples the cable to the driver. The bulk cable current, as well as currents in individual wires, was measured for this excitation mode (other means of excitation, such as through certain pins on the cable connectors, will not be considered with this model). In general, the current in the cable can be expanded in a Fourier series in the azimuthal angle ϕ. In this representation, it is clear that only the n = 0 mode will carry a net current; all the other modes will be proportional to either $\cos(n\phi)$ or $\sin(n\phi)$ and give a net current of zero along any slice of the cable perpendicular to the cable axis. This is called the coaxial excitation mode since it is axisymmetric. The excitation and propagation of this mode needs to be studied, as well as its coupling to the exciter geometry of the satellite tests. The n = 1 mode can be expected to be the most efficiently coupled to the exciting geometry, and so it will be treated as well, although it would not contribute to the bulk current on the cable.

The coupling coefficient is considered first. It is the ratio of the average radial field at the surface of the cable bundle to the field between the capacitive drive plate and the ground. Note that if the system were symmetric, i.e., if the cable were centered between identical drive and ground planes, this coupling would be zero and no net current should be measured at any z-slice (assuming, as has been done in this homogeneous model, that the cable has no azimuthal dependences). The cable is placed midway to the drive plate, which is of the same width as the cable, but the ground plane is wider (taken as effectively infinite below) and the resultant convergence of the field lines causes there to be a net radial electric field at the cable surface. The two-dimensional problem of the capacitor is considered with an infinite ground plane and neglecting the curvature of the system. Also, the influence of the cable on the field structure was neglected because of the assumption that the cable does not conduct azimuthally but only axially. The Schwartz-Christofel conformal mapping solution of the problem of the field between the two plates may be found, for example, in Bewley (Ref. 9), to the approximation that the upper plate is semi-infinite. If H is the distance between plates $Z = X + iY$ the complex coordinate, the edge of the upper plate at $X = 0$, $Y = H$, then in terms of the complex parameter T,

$$Z = h/\pi \ (1 + T + \log T)$$

$$W = -i/\pi \ \log T \qquad (119)$$

where W is the complex potential. A short computer code to evaluate the electric field direction along the surface of the cylindrical cable bundle and to evaluate the average field, using the above results was written. A Newton-Raphson iteration is used to calculate T given Z, from which W and DW/DZ are found. For typical parameters (3 cm width drive plate, 3 cm above RG-19 cable), the coefficient relating the radial electric field to the interplate field is 0.17. Thus, there is a reduction in effective driving by a factor of four due to geometric effects alone.

Note that the theoretical model which predicted 12 A for the tests assumed a triaxial line. Inclusion of this geometric effect would

reduce predicted current to 3A, substantially improving agreement with experiment. Use of this factor, derived from 2-D potential theory, clearly requires the assumption that the dominant mode of current is quasi-Transverse Electromagnetic (TEM). This is plausible as, for ~3 cm spacing between cable and ground plane. The cutoff frequency would be of order $v \sim c/d = 3 \times 10^8/0.03 = 10^{10}$ Hz which would cut-off all other modes of interest. Consequently, in evaluating the integrals over λ, the contribution near $\lambda = 0$ dominates and the use of finite limits ($\lambda \sim 30$ in practice) instead of integrating to $\lambda = \infty$ is quite acceptable.

COAXIAL DRIVER

As noted in the last section solutions for the uniaxial medium problem are, for the azimuthally symmetric case

$$U = \begin{cases} \int_{-\infty}^{\infty} I_0(u\rho)\, e^{-i\lambda z}\, d\lambda \\ \int_{-\infty}^{\infty} K_0(u\rho)\, e^{-i\lambda\rho}\, d\lambda \end{cases}$$

$$u^2 = \frac{\sigma_z}{G}(\gamma^2 + \lambda^2) \qquad (120)$$

for TM waves and

$$V = \begin{cases} \int_{-\infty}^{\infty} I_0(v\rho)\, e^{-i\lambda z}\, d\lambda \\ \int_{-\infty}^{\infty} K_0(v\rho)\, e^{-i\lambda z}\, d\lambda \end{cases}$$

$$v^2 = \frac{\mu_z}{\mu}(\gamma^2 + \lambda^2) \qquad (121)$$

for TE waves. Note that the TEM mode is included as the (singular) limit $\lambda = 0$ of the TM mode. This will allow us to do the integrals over a finite domain (see above).

Figure 12 shows the geometry for the coaxial problem.

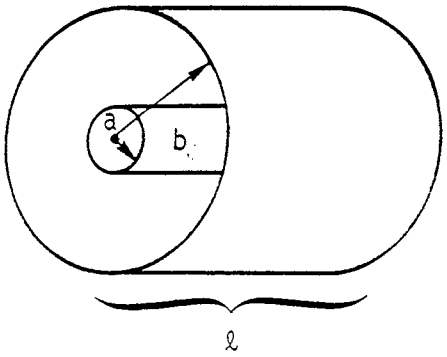

Figure 12. Geometry of coaxial problem.

Inside $\rho = a$ there is a uniaxial cylinder modeling the cable bundle. For $a < \rho < b$ there is free space. At $\rho = b$ there is a conductor to which the exciting voltage is applied. The fields must be continuous across the $\rho = a$ boundary and at $\rho = b$ the transfer fields are zero and the normal electric field is specified. General solutions then are

$$U = \int_{-\infty}^{\infty} A(\lambda)\, I_0(u\rho)\, e^{-i\lambda z}\, d\lambda \tag{122}$$

for $\rho \leq a$, and

$$U = \int_{-\infty}^{\infty} \left(B(\lambda)\, I_0(u\rho) + C(\lambda)\, K_0(u\rho)\right) e^{-i\lambda z}\, d\lambda \tag{123}$$

for $a \leq \rho \leq b$. The driver, E_ρ specified couples only to the TM case, not the TE, so only U is needed for complete specification of the fields. There are three equations required for solution. Three equations have been eliminated through excitation of only TM waves.

Specification of the radial field at $\rho = b$ requires that

$$\int_{-\infty}^{\infty} \left\{-i\lambda U_g\, B(\lambda)\, I_1(u_g b) + i\lambda u_g\, C(\lambda)\, K_1(u_g b)\right\} e^{-i\lambda z}\, d\lambda$$

$$= E_\rho(\rho = b, \omega) \tag{124}$$

$$= \int_{-\infty}^{\infty} f(\lambda)\, e^{-i\lambda z}\, d\lambda \tag{125}$$

where the subscript i indicates variables on the interior of the cable bundle and the g subscript indicates quantities evaluated in the gap between the driver and the cable bundle. The function $f(\lambda)$ may be evaluated by the inverse transform (in λ) of the impressed field E_ρ. The field is uniform in z for $-\ell/2 < z < \ell/2$ and zero elsewhere. Evaluating the integral

$$f(\lambda) = \int_{-\infty}^{\infty} E_\rho(\omega)\, e^{-\lambda z}\, dz = \frac{1}{i\lambda} E(\omega) \left(e^{i\lambda\ell/2} - e^{-i\lambda\ell/2}\right) \tag{126}$$

at $\rho = a$ results in, for the symmetric excitation case, and dropping the integral operators, since the unknown coefficients are required to be specified for all λ. Continuity of H_ϕ

$$-\sigma_i u_i\, A(\lambda)\, I_1(u_i a) + \sigma_g u_g\, I_1(u_g a)\, B(\lambda) = \sigma_g u_g\, K_1(u_g a)\, C(\lambda) \tag{127}$$

and continuity of E_z

$$-(\gamma_i^2 + \lambda^2)\, A(\lambda)\, I_0(u_i a) + (\gamma_g^2 + \lambda^2)\, I_0(u_g a)\, (B(\lambda)$$

$$= -(\gamma_g^2 + \lambda^2)\, C(\lambda)\, K_0(u_g a) \tag{128}$$

These equations may be solved analytically and the determinant of coefficients is

$$\Delta = -i\lambda u_g \left[u_g\sigma_g (\gamma_i^2 + \lambda^2)\, I_0(u_i a) \times \{I_1(u_g b)\, K_1(u_g a)\right.$$

$$\left. - I_1(u_g a)\, K_1(u_g b)\} + u_i\sigma_i(\gamma_i^2 + \lambda^2)\, I_1(u_i a)\, \{I_0(u_g a)\, K_1(u_g b)\right.$$

$$\left. + I_1(u_g b)\, K_0(u_g a)\} \right. \tag{129}$$

The solution for the coefficients is

$$A(\lambda) = f(\lambda)\, \sigma_g u_g\, (\lambda_g^2 + \lambda^2) \left[I_1(u_g a)\, K_0(u_g a) + I_0(u_g a)\, K_1(u_g a)/\right]/\Delta$$

$$= f(\lambda)\, \sigma_g u_g\, (\gamma_g^2 + \lambda^2)/(u_g a \Delta) \tag{130}$$

$$B(\lambda) = [\sigma_i u_i(\gamma_g^2 + \lambda^2)\, I_1(u_i a)\, K_0(u_g a)$$

$$+ \sigma_g u_g(\gamma_i^2 + \lambda^2)\, I_0(u_i a)\, K_1(u_g a)]\, f(\lambda)/\Delta \tag{131}$$

$$C(\lambda) = -\sigma_i u_i(\gamma_g^2 + \lambda^2)\ I_1(u_i a)\ I_0(u_g a)$$

$$+ \sigma_g u_g(\gamma_i^2 + \lambda^2)\ I_1(u_g a)\ I_0(u_i a) \qquad (132)$$

The current induced on the cable bundle is the interesting quantity in this case

$$J_z(\rho,\omega) = -\sigma_{zi}(-\gamma_i^2 + \lambda^2)\ U$$

$$= -\sigma_z(\gamma_i^2 + \lambda^2) \int_{-\infty}^{\infty} A(\lambda)\ I_0(u_i\rho)\ e^{-i\lambda z}\ d\lambda \qquad (133)$$

The total bundle current I_b may be found by integrating the current density

$$I_b = 2\pi \int_0^a J_z(\rho,\omega)\ \rho\, d\rho$$

Using the high frequency approximations for the Bessel functions it is found that the current density goes as the $\omega^{3/2}$ times the driving waveform, i.e., the derivatives of the driver plays a part in the high frequency response. Since the response will have a faster rising response than the driver filtration of waveform by the sensors will likely play a part.

COAXIAL DRIVER DISCUSSION

Figure 13 shows the assumed time dependence of the drive electric field E(t) between the plate. This E(t) does not have vanishing first and second derivates at t = 0. Because the response function behaves as $\omega^{3/2}$, it was felt desirable to see how a less-sharply increasing function of time would behave. Figure 14 shows a modified E(t) with vanishing first and second derivatives with respect to time at t = 0. Using the results above and doing the radial integration by Simpson's rule over a few skin depths into the cable bundle give the results shown in Figures 14 through 17. The concept of skin depth has the usual meaning here. Since there are a range of frequencies and consequently no unique skin depth, the integration limits were chosen as a function of frequency. The integration over λ is done by Simpson's rule, the principal part of the integral being determined by deforming the contour above the origin. The limits on λ are taken as ± 30. Both these limits and the size

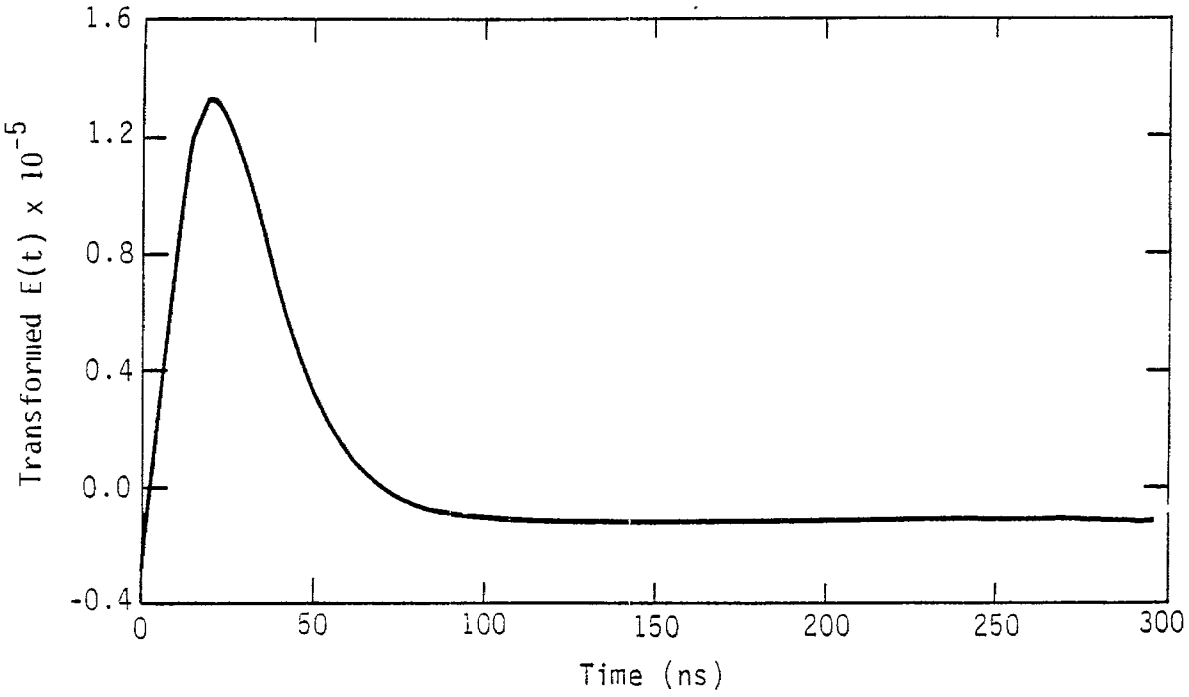

Figure 13. Electric field drive as a function of time.

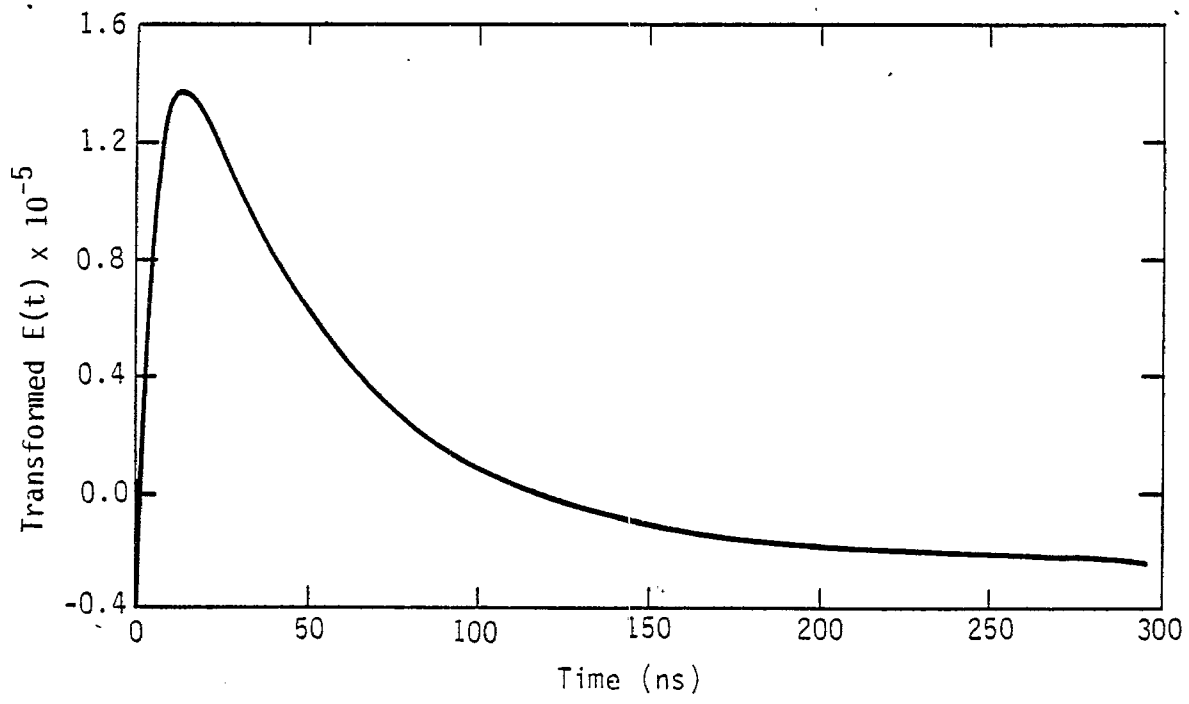

Figure 14. Modified electric field drive as a function of time. The first and second derivatives of E with respect to time are zero. Otherwise, E(t) is similar to the standard case of Figure 13.

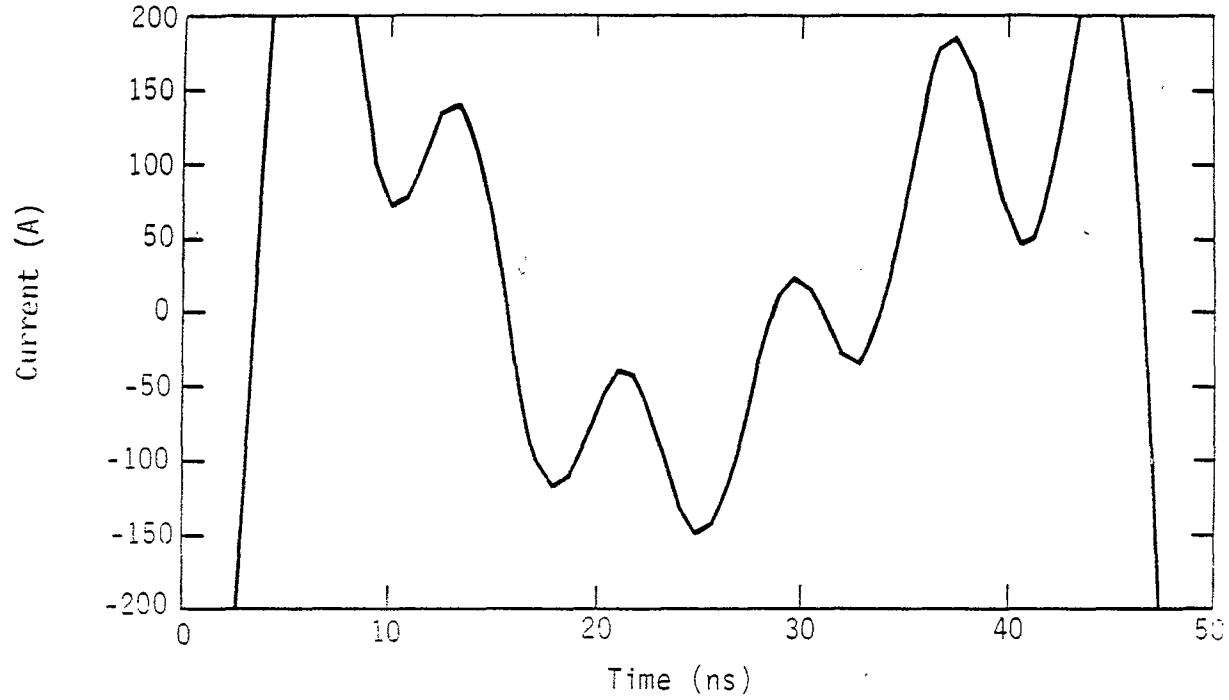

Figure 15. Bulk cable current for the drive field E(t) of Figure 13.

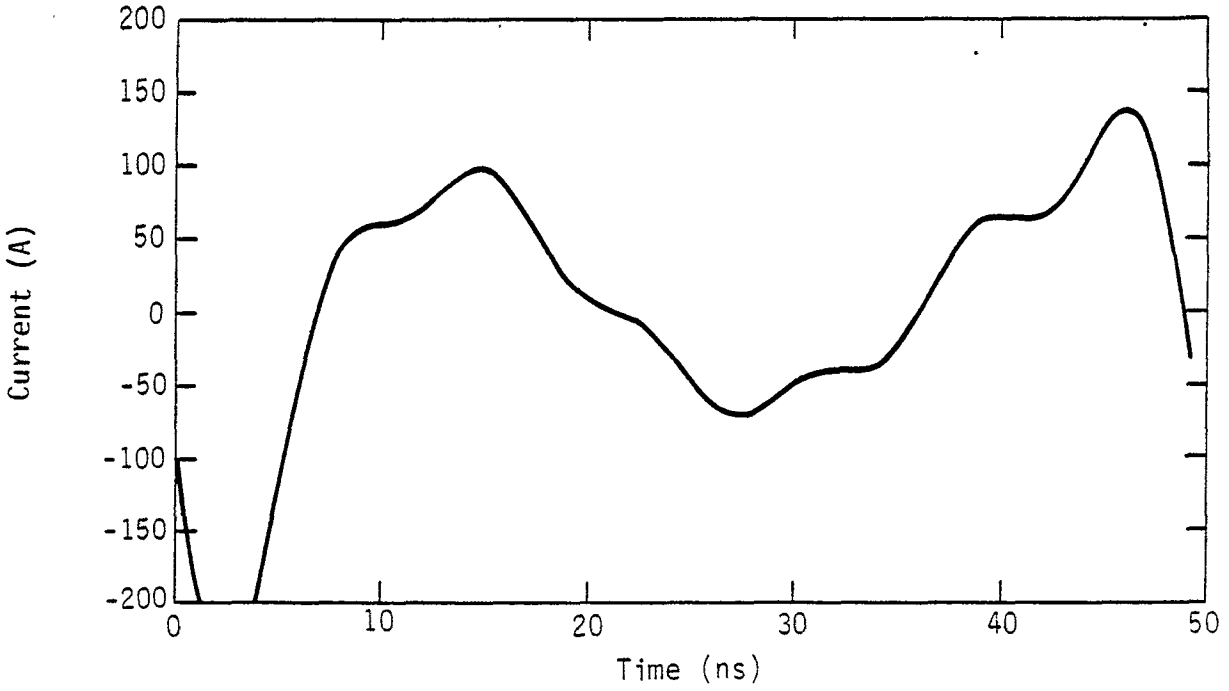

Figure 16. Bulk cable current for the drive field E(t) of Figure 14.

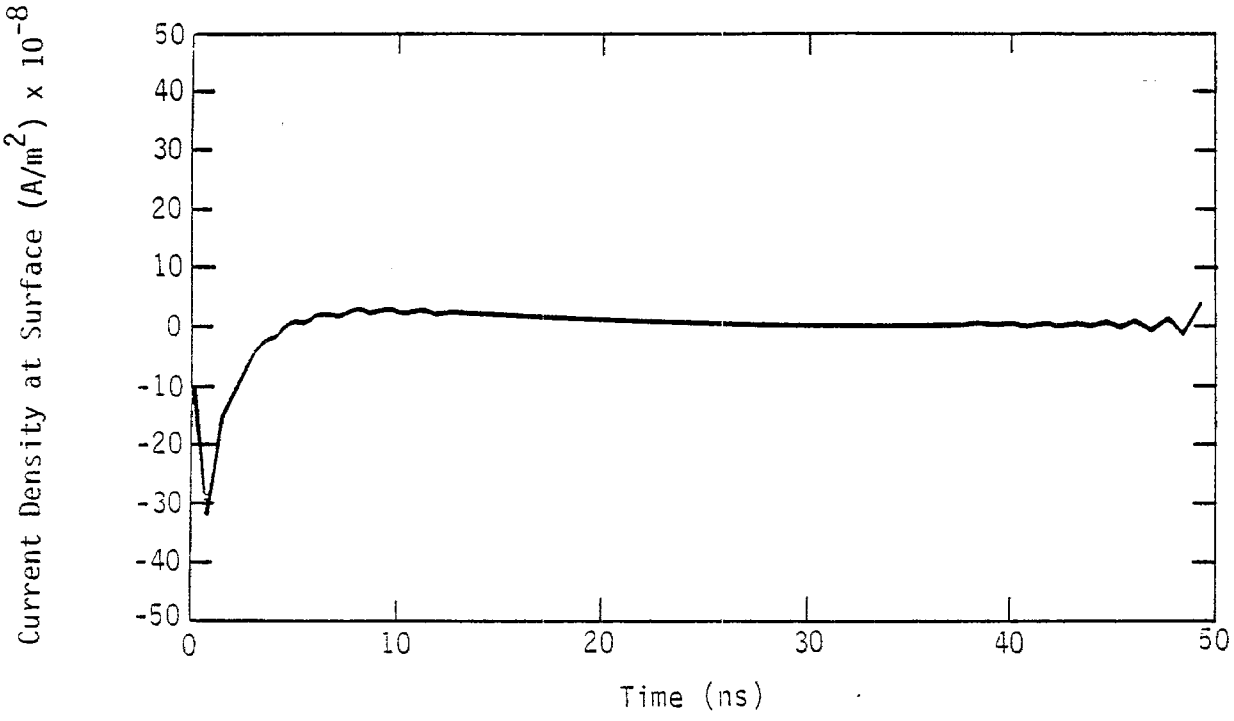

Figure 17. Surface current density for the drive E(t) of Figure 13.

of the detour above the origin have been varied and the answers are not sensitive to these parameters.

Expected currents were about 12 A, with measured currents about an order of magnitude below this (~2 A). The first figures plot the two drive fields used. Bulk current predictions are shown in Figures 14 and 15 for the two E(t). Figures 17 and 18 display the respective surface current densities. The results are somewhat higher than observations. This is not due to neglect of differential-mode (as opposed to common-mode) currents, as the predictions are above those of ~12 A max based purely on triaxial line, common mode currents. However, line reflections and characteristic impedances are neglected (cable is assumed floating). It is probably the complex interactions of such mismatches and reflections which account for the overestimate of current magnitude (the triaxial line mode explicitly includes characteristic impedances of cable, drive coax, and transfer admittances and impedances). Note also that the fact that modes may be cut off and attenuate exponentially the drive is not explicitly accounted for. Qualitatively, the behavior is correct except for an excessive presence of lower frequency components, superimposed

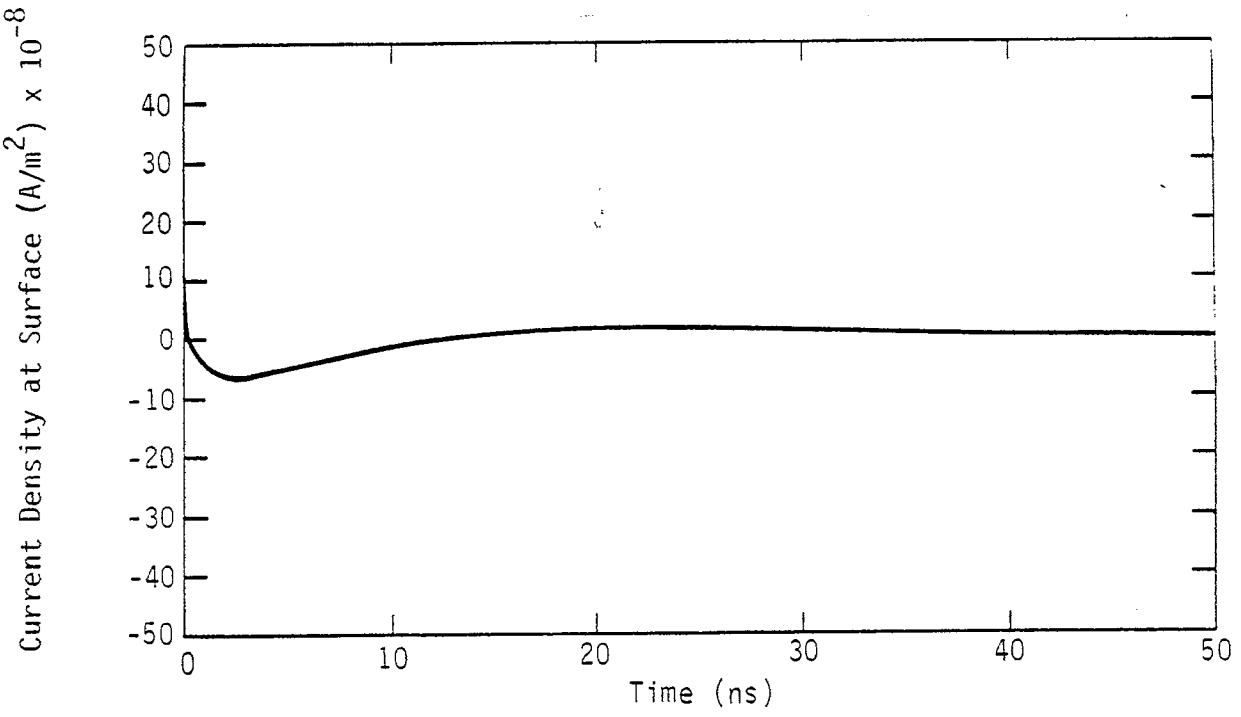

Figure 18. Surface current density for the drive E(t) of Figure 14.

on the ~10^{-8} s period (100 MHz) ringing of the line. This frequency is selected by the length of the driven section of the line, 1.5 m, which is one-half wavelength. Note also the strong dependence on the details of the pulse shape.

It is plausible that our model overestimates observed signal amplitude, particularly lower frequency components, because these TM components are cut off and damp exponentially with distance between the sensor and the region of excitation. This is suggested as well by the fact that the simple transmission-line model which considers only the differential-mode TEM signal is of smaller amplitude (~12 A) and does not contain the lower frequency baseline shift as contained in this model. Depending upon the boundary conditions of interest in the actual SGEMP problem, analysis of the TEM mode only, with appropriate termination conditions, could be the most appropriate model.

To test the role of the cutoff of the TM modes, the integrand multiplied by $\exp(K_{atten}Z_s)$, where $Z_s = 0.4$ is the distance between the current sensor and the drive strip, and

$$K_{atten} = \max \left(0, \quad \frac{1}{\lambda^2} - \frac{1}{d^2}\right) \tag{134}$$

where d = 3 cm is the guide wavelength. The results are shown in the accompanying figures. Figures 19 and 20 give the bulk cable currents as seen at the sensor for the drive electric fields of Figures 13 and 14, and may be contrasted to the currents shown in Figures 16 and 18. Similarly, Figures 21 and 22 give the corresponding surface current densities. Agreement with experiment has been improved considerably. A detailed treatment of the mode structure beyond the strip should probably further improve agreement.

PARALLEL PLATE DRIVER

The parallel plate driver case is much more complex than the coaxial driver problem because the azimuthal symmetry is broken. Further both E_ρ and E_ϕ fields are specified and nonzero which provide contributions to the fields from both TE and TM solutions. In this simple model, the parallel plate driver is modeled by a specification of a uniform y-directed electric field E_y at a distance $\rho = b$ from the center of the cable bundle. From E_y, both E_ρ and E_ϕ are specified; as well as E_z is required to be zero. The specified fields E_ρ and E_ϕ will be represented in the λ transform space as $f(\lambda)$ and $g(\lambda)$ respectively. Again the fields are required to be continuous across the $\rho = a$ boundary of the cable bundle. The potentials are

$$U = \sum_n \int_{-\infty}^{\infty} A_n(\lambda)\, I_n(u_i\rho)\, e^{-in\phi}\, e^{-i\lambda z}\, d\lambda$$

$$V = \sum_n \int_{-\infty}^{\infty} R_n(\lambda)\, I_n(v_i\rho)\, e^{-in\phi}\, e^{-i\lambda z}\, d\lambda \tag{135}$$

for $\rho \leq a$, and

$$U = \sum_n \int_{-\infty}^{\infty} [B_n(\lambda)\, I_n(u_g\rho) + C_n(\lambda)\, K_n(u_g\rho)]\, e^{-in\phi}\, e^{-i\lambda z}\, d\lambda$$

$$V = \sum_n \int_{-\infty}^{\infty} [S_n(\lambda)\, I_n(v_g\rho) + T_n(\lambda)\, K_n(v_g\rho)]\, e^{-in\phi}\, e^{-\lambda z}\, d\lambda \tag{136}$$

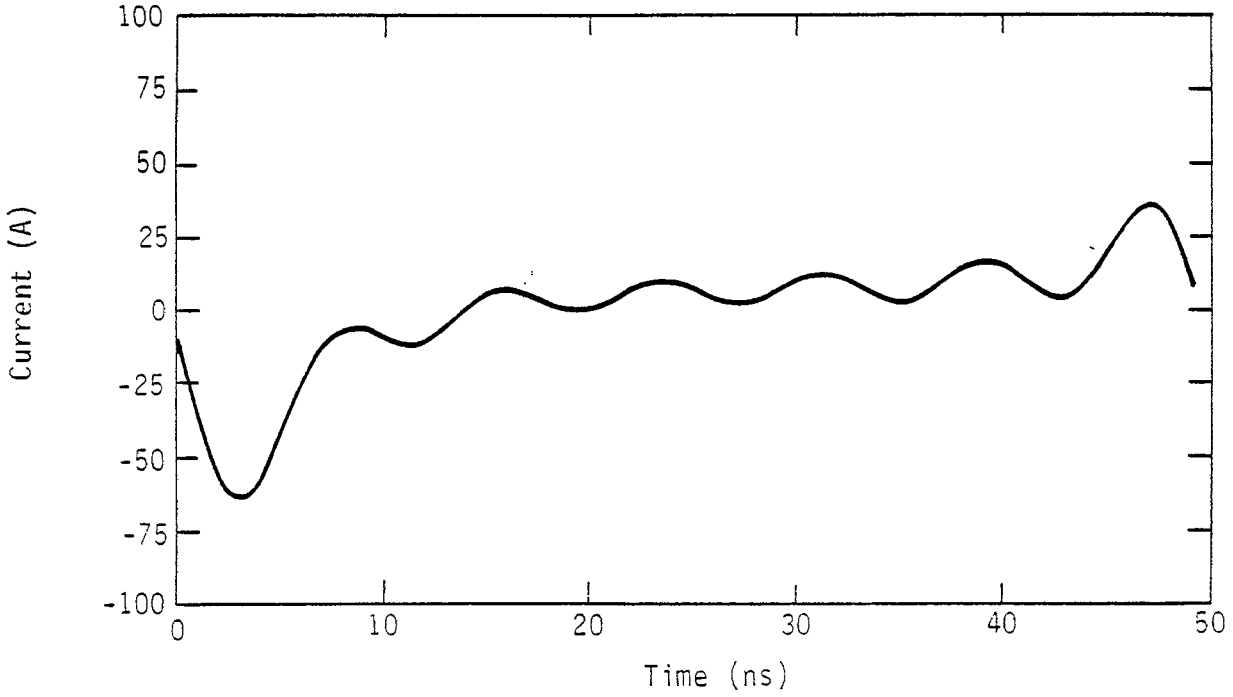

Figure 19. Bulk cable current, E(t) as in Figure 13, as seen by sensor. Attenuation of TM modes has been taken into account. Compare with Figure 15, which gives unattenuated current.

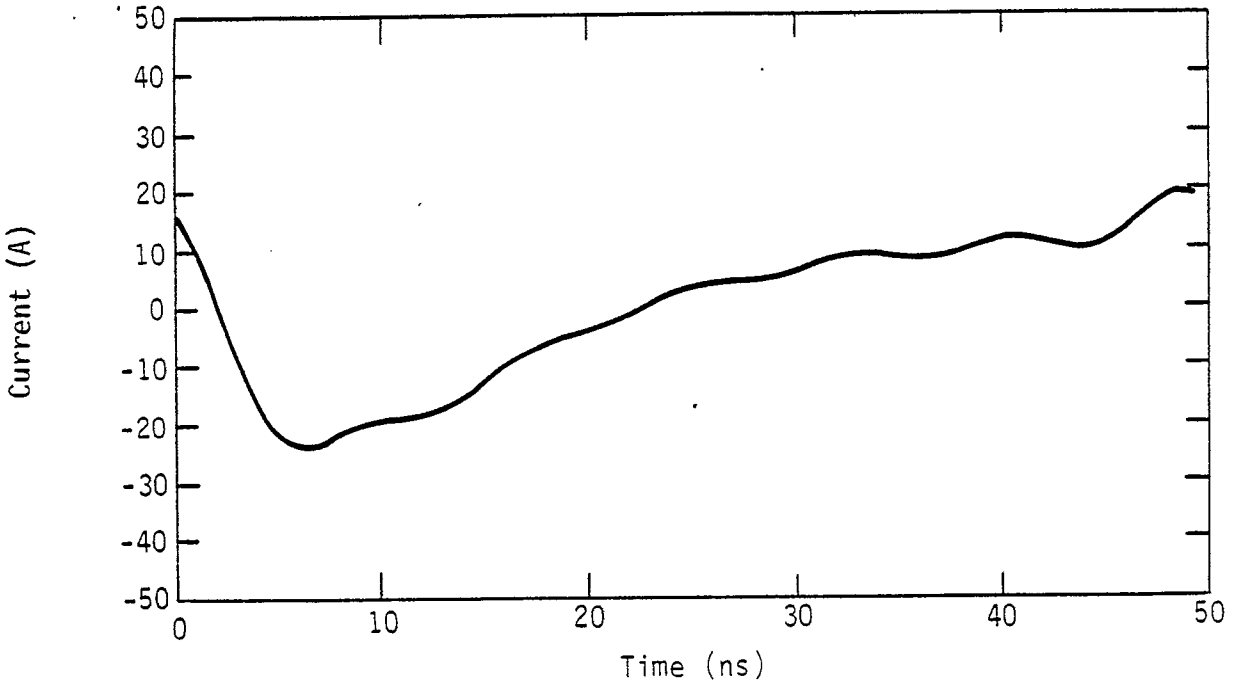

Figure 20. Bulk cable current, E(t) of Figure 14, as seen by sensor. Attenuation of TM modes has been taken into account. Compare with Figure 16, which gives unattenuated current.

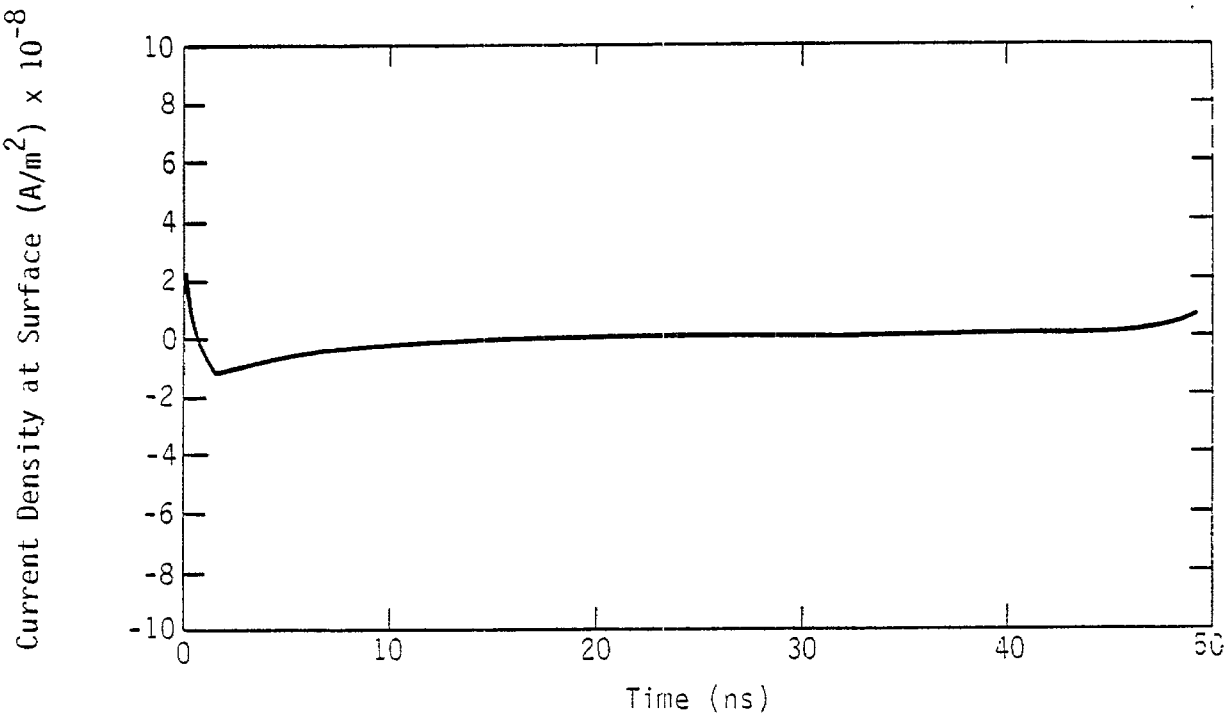

Figure 21. Bulk cable current as in Figure 16, but with attenuation of TM modes beyond the drive strip accounted for.

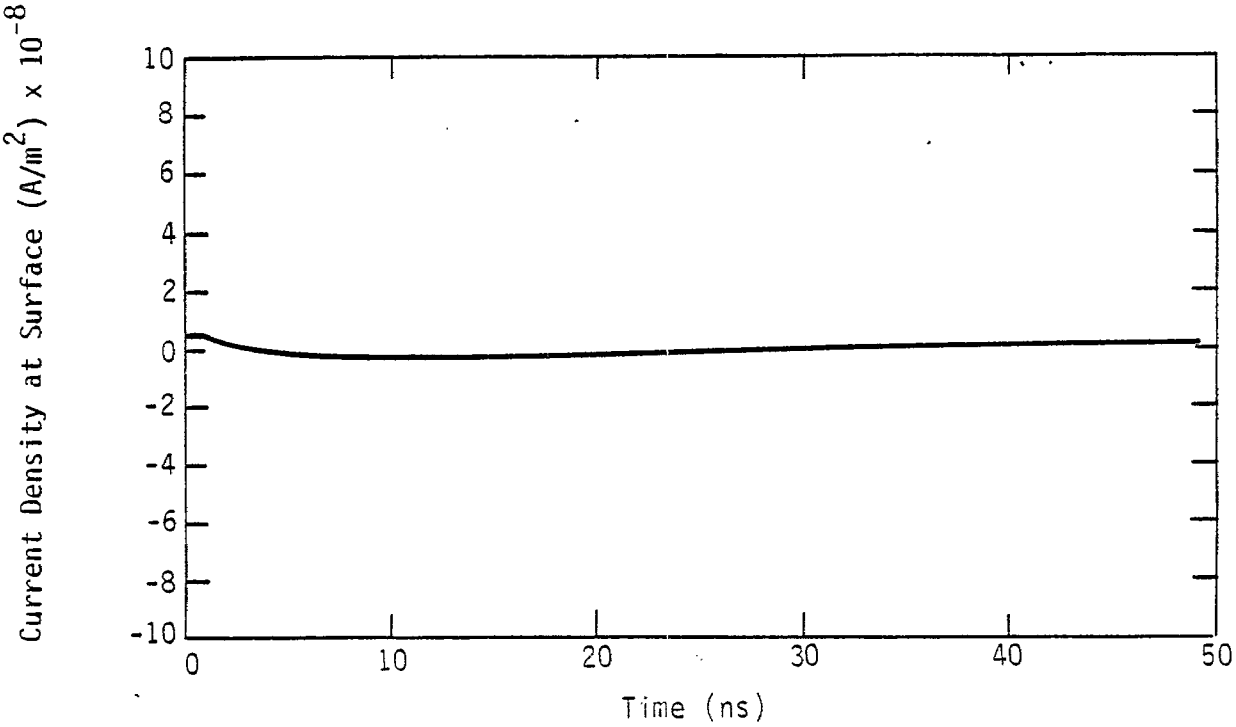

Figure 22. Bulk cable current as in Figure 18, but with TM mode attenuation between the drive strip and sensor accounted for.

for $a \leq \rho \leq b$. Specification of the fields at $\rho = b$ yields, dropping the integral operators and suppressing the $e^{in\phi}\, e^{i\lambda z}$ factors

$$-i\lambda u_g \left[B_n(\lambda)\, I_n^1(u_g b) + C_n(\lambda)\, K_n^1(u_g b)\right]$$

$$- \frac{\omega n}{\rho} \left[S_n(\lambda)\, I_n(u_g b) + T_n(\lambda)\, K_n(u_g b)\right]$$

$$= f_n(\lambda) \qquad (137)$$

specifying E_ϕ

$$- \frac{n\lambda}{\rho} \left[B_n(\lambda)\, I_n(u_g b) + C_n(\lambda)\, K_n(u_g b)\right.$$

$$\left. + \frac{i\omega u_g}{} \; u_g \left[S_n(\lambda)\, I_n^1(v_g b) + T_n(\lambda)\, K_n^1(v_g b)\right.\right.$$

$$= g_n(\lambda) \qquad (138)$$

and finally specifying E_z

$$-\left(\gamma_g^2 + \lambda^2\right) \left[B_n(\lambda)\, I_n(u_g b) + C_n(\lambda)\, K_n(u_g b)\right] = 0 \qquad (139)$$

For the interface of $\rho = a$ all fields must be continuous

E_z:

$$-\left(\gamma_g^2 + \lambda^2\right) A_n(\lambda)\, I_n(u_i a) = -\left(\gamma_g^2 + \lambda^2\right)\left[B_n(\lambda) I_n(u_g a)\right.$$

$$\left. + C_n(\lambda)\, K_n(u_g a)\right] \qquad (140)$$

H_z:

$$-\left(\gamma_i^2 + \lambda^2\right) R_n(\lambda)\, I_n(v_i a) = -\left(\gamma_g^2 + \lambda^2\right)\left[S_n(\lambda) I_n(v_g a)\right.$$

$$\left. + T_n(\lambda) K_n(v_g a)\right] \qquad (141)$$

E_ρ:

$$-i\lambda i_g i\, A_n(\lambda)\, I_n^1(u_i a) - \frac{\omega n \mu}{\rho}\, I_n(v_i a)\, R_n(\lambda)$$

$$= -i\lambda u_g \left[B_n(\lambda)\, I_n^1(u_g a) + C_n(\lambda)\, K_n(u_g a)\right]$$

$$- \frac{wn\mu}{\rho} \left[S_n(\lambda)\ I_n(v_g a) + T_n(\lambda)\ K_n(v_g a) \right] \qquad (142)$$

For this case the current density is

$$J_z = \sigma_z E_z = \sum_n \int_{-\infty}^{\infty} A_n(\lambda)\ I_n(u_i \rho)\ e^{-in\phi}\ e^{-i\lambda z}\ d\lambda \qquad (143)$$

where the sum over n has contribution as required by the ϕ variation of E_ρ, E_z. For the flat plate case, $n = \pm 1$ is sufficient to determine the fields since $E_\rho(\rho,\phi) = E_\rho(\rho) = E_\rho(\rho) \cos\phi$ and $E_\phi(\rho,\phi) = E_\phi(\rho) \sin\phi$. The coefficient $A(\lambda)$ may be found by numerical solutions to the 6 x 6 set of linear equations and numerical performing the λ integ-ations. In addition to $A_n(\lambda)$, which is required for the current density, the other 5 coefficients are useful to keep a running check on the boundary conditions. Truncation errors and errors in function evaluation sometimes lead to inconsistent solutions, which must be considered.

EQUATIONS FOR N = 1 MODE

The N = 1 case was modeled using the equations derived above. The matrix of coefficients was solved numerically. Asymptotic values for the Bessel functions and their ratios were used when appropriate for numerical convenience. The results are qualitatively similar to the results for the N = 0 case. Figures 23 and 24 show typical surface current density profiles (note that this would have to be multiplied by cos ϕ to get the current distribution over the bundle). These may be compared to the similar results for the n = 0 mode in Figures 17 and 18. This enables qualitatively discussion of the relationship between bulk and individual wire currents. Since the skin depth of drive frequencies of most interest is $\approx 10^{-5}$ m, much less than wire diameters, the currents carried by the wires may be estimated by their fraction of the surface area. The minimum and maximum currents are then proportional to $\left|J(n=0,\ r=0) + J(1,1)\right|$ and $\left|J(0,0) - J(1,1)\right|$.

Note that the peak current density at the bundle surface for the n = 1 is 33 to 50 percent of that of the n = 0 mode, depending upon which pulse shape is assumed. This suggests a possible 3:1 variation in wire currents. Because an individual wire wanders through the bundle, considerable variation might be expected.

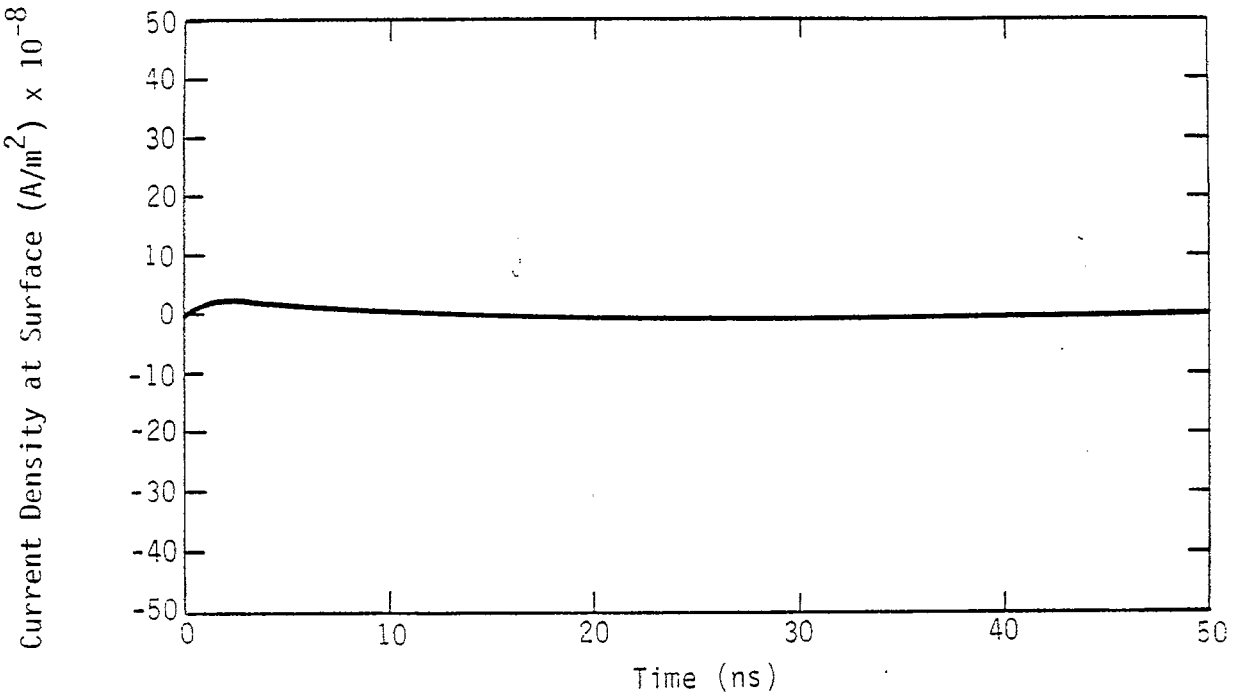

Figure 23. Surface current density in the n=1 mode on the cable for the drive E(t) of Figure 13.

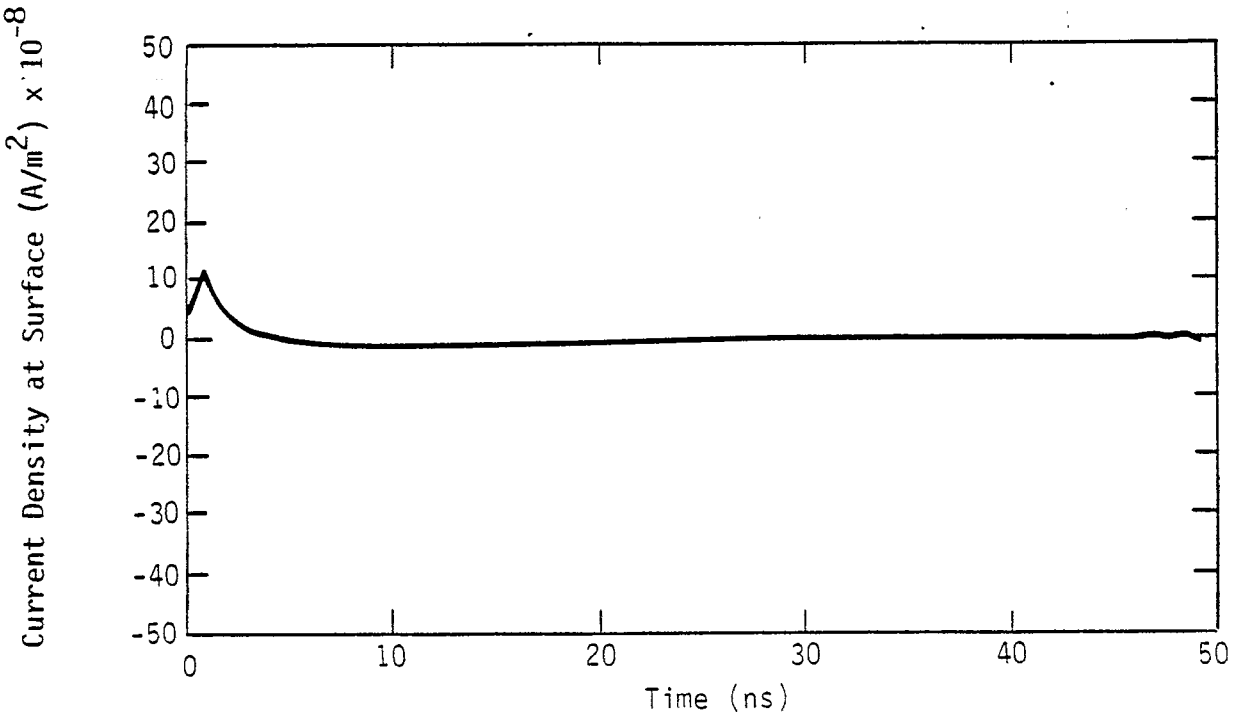

Figure 24. Surface current density in the n=1 mode on the cable for the drive E(t) of Figure 14.

VIII. CONCLUSIONS

There are three basic problems addressed in the report:

(1) Distribution of currents on a bundle of shielded wires.

(2) Perturbation of measurements by sensors,

(3) Explanation of differences in predictions for bulk currents for complex a d simple bundles.

Solutions of the propagation of signals down a uniform cable bundle are given in both the time and frequency domains. For both solutions, it is concluded that, by far, the majority of the current is carried in wires on the surface of the bundle and that very little current diffuses to the interior.

Calculations of the effect of pulling a wire out to place a sensor around it show a substantial perturbation to the current distribution for a typical bundle. These calculations should be followed by experimental verification and use of termination impedances appropriate to other systems.

The third part of the report describes very detailed calculations of the coupling of parallel plate and coaxial drivers to a uniaxial cable bundle. Models of the two drivers were constructed and bulk currents predicted. Agreement with experiment was not too bad. The concept of coupling coefficient for the coaxial mode drive from the departure of the parallel plate driver from the perfect configuration was particularly useful in explaining the various experimental results.

APPENDIX A

TIME DOMAIN PROPAGATION OF A SIGNAL ALONG A BUNDLE

Consider the multiconductor transmission line equations

$$L \frac{\partial I}{\partial t} + \frac{\partial V}{\partial z} + R\ I = E_z^{inc} \tag{A1}$$

$$C \frac{\partial V}{\partial t} + \frac{\partial I}{\partial z} + G\ V = 0 \tag{A2}$$

Important relations are

$$L \cdot C = 1/v^2 \tag{A3}$$

which is a statement of our requirement, for the moment, that all waves travel at the same velocity and

$$G = \frac{f\sigma}{\varepsilon} C \qquad f \leq 1$$

which is a statement of the assumptions that the conductance is proportional to the capacitance, but is dominated by the capacitive terms. These equations may be written with current and charge varying using

$$Q = C\ V$$

$$\frac{\partial I}{\partial t} + v^2 \frac{\partial Q}{\partial z} + L^{-1} R\ I = L^{-1} E_z \tag{A4}$$

where R is assumed diagonal. Changing to retarded time

$$\tau = vt - z$$

$$z' = z$$

$$\frac{\partial}{\partial z} = \frac{\partial}{\partial z'} \frac{\partial z'}{\partial z} + \frac{\partial}{\partial \tau} \frac{\partial \tau}{\partial z} = \frac{\partial}{\partial z'} - \frac{\partial}{\partial \tau}$$

$$\frac{\partial}{\partial \tau} = \frac{\partial}{\partial z'} \frac{\partial z'}{\partial \tau} + \frac{\partial}{\partial \tau} \frac{\partial \tau}{\partial \tau} = v \frac{\partial}{\partial \tau} \tag{A5}$$

and four forward (F) and backward (B) going waves,

$$F = I + vQ \qquad I = \frac{F + G}{2}$$

$$G = I - vQ \qquad Q = \frac{F - G}{2v} \tag{A6}$$

The transmission line equations are now, dropping the prime z.

$$\frac{\partial G}{\partial \tau} + \frac{\partial}{\partial z}\frac{(F - G)}{2} + L^{-1} R \frac{F + G}{2v} = \frac{L^{-1}}{v} E_z$$

$$- \frac{\partial G}{\partial \tau} + \frac{\partial}{\partial z}\frac{(F + G)}{2} + \frac{f\sigma}{v\epsilon} \frac{F - G}{2} = 0 \qquad \text{(A7)}$$

Simplifying

$$\frac{\partial F}{\partial z} + L^{-1} R \frac{F + G}{2v} + \frac{f\sigma}{v\epsilon} \frac{F - G}{2} = \frac{L^{-1}}{v} E_z$$

$$2\frac{\partial G}{\partial \tau} - \frac{\partial G}{\partial z} + L^{-1} R \frac{F + G}{2v} - \frac{f\sigma}{v\epsilon} \frac{F - G}{2} = \frac{L^{-1}}{v} E_z \qquad \text{(A8)}$$

Looking only at a long line and considering only waves in one direction, i.e., G = 0, then

$$\frac{\partial F}{\partial z} = - \frac{L^{-1}R}{2v} F - \frac{f\sigma}{2v\epsilon} F$$

$$= - \frac{vRC}{2} F - \frac{f\sigma}{2\pi\epsilon} F \qquad \text{(A9)}$$

Comparing the equations $Q = CV$ and $\nabla^2 V = \rho/\epsilon_0$ shows that the operation $L^{-1} = v^2 C$ looks very much like the Laplacian. If ρ is the central point and ρ_i are the six external points, C_d is the value of the diagonal elements and $-C_{od}$ is the value of the off-diagonal elements ($C_{od} > 0$) then the charge or the central element is

$$Q = - C_{od}(\sum V_{ei} - GV_\rho) \qquad \text{(A10)}$$

The Laplacian is

$$\nabla_\perp^2 V = \frac{1}{Gb^2} (\sum V_{ei} - GV_\rho) \qquad \text{(A11)}$$

as can be shown by inserting

$$V = x^2$$

$$\nabla_\perp^2 V = 2 = \frac{1}{Gb^2} [b^2 \times 4 + (2b)^2 \times 2] \qquad \text{(A12)}$$

and

$$V = y^2$$

$$\nabla_{\perp}^2 V = 2 = \frac{1}{Gb^2} \left[(\sqrt{3}\, b)^2 \times 4\right] \tag{A13}$$

so that $C \rightarrow -Gb^2\, C_{od}\, \nabla_{\perp}^2$ for interior wires. For the exterior the self capacitance terms to ground dominate and

$$\frac{\partial F}{\partial z} = 3vb^2\, R\, C_{od}\, \nabla_{\perp}^2 - \frac{f\sigma}{2v\epsilon}\, F \tag{A14}$$

Going entirely over the continium limit

$$F = J + v\rho$$

$$G = J - v\rho \tag{A15}$$

where

$$J = I/A \tag{A16}$$

and

$$\rho = Q/A \tag{A17}$$

where A is the unit cell area, i.e.,

$$A = 3\sqrt{3}\, b^2 \tag{A18}$$

The above differential Equation A13 is a diffusion equation. For the nearest neighbor approximation, the interwire capacitance is of the order $C_{od} \approx 10^{-11}$ F/m. The diffusion coefficient, D, is

$$D = 3vb^2\, R\, C_{od} \sim (3)\,(3 \times 10^8)\left(10^{-3}\right)^2 (0.2)(10^{-10})$$

$$\sim 2 \times 10^{-8}\ \text{m}$$

Therefore to diffusion 1 mm into the bundle requires propagation along the bundle of 50 m, so little diffusion occurs into cables that are a few meters long.

APPENDIX B

ANALYTIC PULSAR WAVEFORMS AND SPECTRA

A difficulty in problems of this type is a choice of a function approximating a driving waveform. A waveform with the following characteristics is required

(1) The function must have fast but smooth rise and slower decay.

(2) The function and its derivative must be 0 at t = 0.

(3) The function must have an analytic Fourier transform.

These combinations may be satisfied by a combination of functions of the form

$$f(t) = \frac{e^{-\alpha t}}{1 + Ge^{-\beta t}} \tag{B1}$$

This function may have zero derivative at t = 0 with the proper choice of G, but has nonzero value there. Therefore two of these functions with the same G coefficient but different exponential coefficients are required for zero value at t = 0. The G coefficient may be found by solving

$$f'(\theta) = \frac{-\alpha e^{-\alpha t}}{1 + Ge^{-\beta t}} + \frac{\beta G e^{-\alpha t} e^{-\alpha t}}{\left(1 + Ge^{-\beta t}\right)^2} \Bigg|_{t=0} = 0 \tag{B2}$$

The result is

$$G = \left(\frac{\beta}{\alpha} - 1\right)^{-1} \tag{B3}$$

G then depends only on the ratio of coefficients. A complete form for the function we are looking for is

$$g(t) = \frac{e^{-\alpha t}}{1 + Ge^{-\beta t}} - \frac{e^{-\alpha t}}{1 + Ge^{-\delta t}} \quad U(t) \tag{B4}$$

where

$$G = \left(\frac{\beta}{\alpha} - 1\right)^{-1} \tag{B5}$$

and

$$\frac{\beta}{\alpha} = \frac{\delta}{\gamma} \tag{B6}$$

and U(t) is the unit step function. This function should look very much like double exponential, except at very early times then the ratio $\beta/\alpha = 10$ is a good choice, which leads to $G = 1/\rho$.

Satisfying condition (3) for an analytic Fourier transform requires that the following integral be solved

$$F(\omega) = \int_0^\infty \frac{e^{-\alpha t}}{1 + Ge^{-\beta t}} e^{-i\omega t} dt \tag{B7}$$

Since $G < 1$ for this problem, the denominator may be expanded in a power series

$$F(\omega) = \int_0^\infty e^{-(\alpha+i\omega)t} \sum_{n=0}^{\infty} (-G)^n e^{-n\beta t} dt$$

$$= \sum_{n=0}^{\infty} (-G)^n \int_0^\infty e^{-(\alpha+n\beta+i\omega)t} dt$$

$$= \sum_{n=0}^{\infty} \frac{(-G)^n}{\alpha + n\beta + i\omega} \tag{B8}$$

In practice the series requires only a few terms for evaluation for G.

REFERENCES

1. Marin, L., E-3A EMP Dipole Test, Volume I, Summary of Test Data and Major Conclusions, Part 1, AFWL-TR-79-90, pg. 85, Air Force Weapons Laboratory, Kirtland Air Force Base, NM, May 1980.

2. Wait, J. R., "Electromagnetic Response of an Anisotropic Conducting Cylinder to an External Source, Radio Science, 13, No. 5, 789-792, September/October 1978.

3. Harrington, R. F., Time Harmonic Electromagnetic Fields, McGraw-Hill, New York, 1961.

4. Agrawal, A. K., H. M. Fowles, L. D. Scott, S. H. Garbaxani, "Application of Modal Analysis to the Transient Response of Multiconductor Transmission Lines with Branches," IEEE Trans. EMC, EMC-21, 256, August 1979.

5. Jackson, J., Classical Electromagnetics, 2nd Edition, John Wiley, 1975, p. 56.

6. King, R. W. P., "Transmission-Line Theory," pp. 25ff, Dover, New York, NY, 1965.

7. Frankel, S., Multiconductor Transmission Line Analysis, Artec House, Menlo Park, CA, pp. 92-93, 1977.

8. Ramo, S., J. R. Whinnery, and T. Van Duzer, Fields and Waves in Communication Electronics, John-Wiley, 1965, p. 436, (Fig. 8.05).

9. Bewley, L. V., Two-Dimensional Fields in Electrical Engineering, Dover Publications, New York, pp. 123ff, 1948.